FE-1749-8
Dist. Category UC-90C

MATERIALS RESEARCH FOR CLEAN UTILIZATION OF COAL

QUARTERLY PROGRESS REPORT
July 1976

Samuel J. Schneider
Project Manager

Institute for Materials Research
National Bureau of Standards
Washington, D. C. 20234

PREPARED FOR THE UNITED STATES
ENERGY RESEARCH AND DEVELOPMENT ADMINISTRATION

Under Contract No. 14-32-0001-1749

Schneider, S. J., Materials research for clean utilization of coal. Quarterly progress Report July 1976, Energy Research and Development Administration FE-1749-8, 73 pages (Available from the National Technical Information Services, Springfield, Va 1976).

313

TABLE OF CONTENTS

I. OJBECTIVE AND SCOPE OF WORK

Coal Gasification processes require the handling and containment of corrosive gases and liquids at high temperature and pressures, and also the handling of flowing coal particles in this environment. These severe environments cause materials failures which inhibit successful and long-time operation of the gasification systems. The project will entail investigations on the wear, corrosion, chemical degradation, fracture, and deformation processes which lead to the breakdown of metals and ceramics currently being utilized in pilot plants (and suffering failures). Studies will also be carried out on new candidate materials considered for improved performance. Special emphasis will be devoted to the development of test methods, especially short-time procedures, to evaluate the durability of materials in the gasification environments. These methods will focus on wear, impact erosion, stress corrosion, strength, deformation, slow crack growth and chemical degradation of refractories. Failure analysis of gasifier components, both metal and ceramic will be conducted as necessary. Failure reports from gasifiers will be compiled, abstracted and recommendations made to ERDA as to the appropriate action to be taken. All studies will be correlated with field inspections and failure analysis on in-service materials. Active consultation and proposal review services to ERDA and associated contractors will be provided.

II. SUMMARY OF PROGRESS TO DATE

The summary of progress is contained in the individual task progress and plans - Section III. See Performance Chart following.

PERFORMANCE AS OF July 1, 1976*

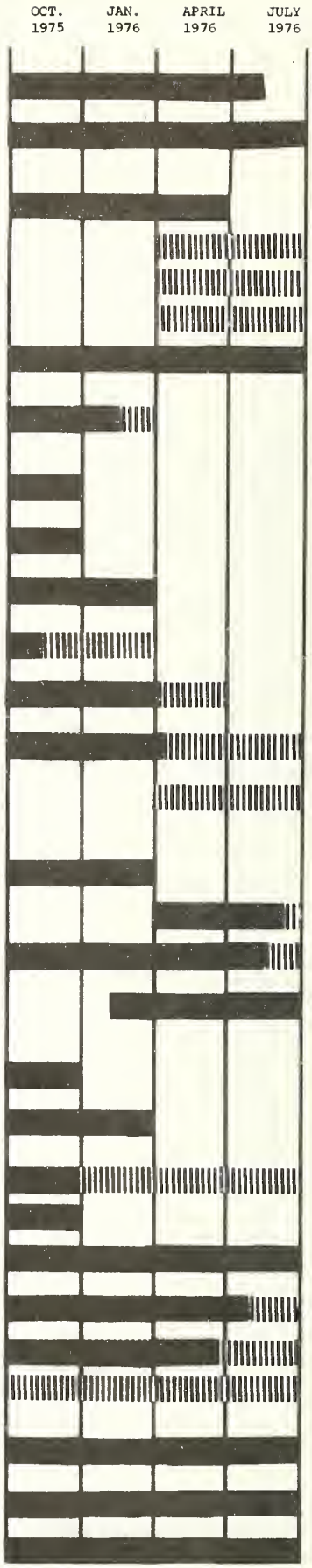

Metal Corrosion

Complete evaluation of the constant strain rate technique with a system of known susceptibility to SCC.

Begin evaluation of the constant strain rate technique with materials and environments of relevance to coal conversion technology.

Metal Wear

Characterize surface films and coatings on test specimens.

Conduct study of sulfide environment effects.

Examine effects of high pressure on erosion/corrosion.

Obtain and examine in-service specimens.

Develop and quantify erosion test method and equipment.

Ceramic Deformation and Fracture

Design controlled atmosphere apparatus for mechanical property measurements in reactive gases at elevated temperatures and elevated pressures.

Measure strength of calcium-aluminate-bonded refractory castable after exposure to elevated-pressure steam at temperatures from 100 to 510°C.

Identify hydration phases of calcium aluminate after exposure to elevated-pressure steam at temperatures from 100 to 510°C.

Measure strength in candidate refractories as a function of loading rate to failure at elevated temperatures without reactive environments.

Construct controlled atmosphere apparatus for mechanical property measurements in reactive gases at elevated temperatures and elevated pressures.

Collect compressive creep data of candidate refractories at elevated temperatures without reactive environments.

Correlate slow-crack-growth, strength, and creep behavior in the absence of reactive environments.

Collect strength data in reactive gases at elevated temperatures and elevated pressures.

Erosive Wear Ceramics

Erosive wear of calcium aluminate bonded alumina-dependence of wear on temperature, velocity and impingement angle.

Erosive wear of other generic castable refractories.

Design and construction of improved apparatus to investigate wear in controlled environments.

Erosive wear study of refractories that have been exposed to high pressure steam.

Chemical Degradation of Ceramics

Assessment of pertinent published phase equilibrium diagrams.

Development of rough screening tests.

Chemical attack of slag
a. commercial refractories
b. controlled laboratory specimens

Assessment of gas-refractory reactions.

Equilibrium studies of the $CaO-Al_2O_3-H_2O$ system in the P and T regions of interest in coal gasifiers.

In conjunction with mechanical properties section correlate chemical stability, strength with phase assemblage.

Determine phase assemblage for laboratory specimens.

Obtain in service specimens and examine phase assemblage.

Proposal Evaluation and Consultation

Participate in ERDA program reviews.

Failure Analysis - Metals and Ceramics

Abstract failure analysis reports made to ERDA and recommend appropriate action. as needed.

Conduct failure analysis on components from coal conversion plants as needed.

*Solid bar refers to percent completed.

III. DETAILED DESCRIPTION OF TECHNICAL PROGRESS

1. Durability and Reliability of Materials of Construction

A. Metals

a) Corrosion (G. M. Ugiansky and C. E. Johnson, 312.04)

Progress: Work has continued with the testing of 310 stainless steel. The constant strain rate technique has been shown to be useful for detecting embrittlement of 310 SS at 1000°F which is dependent on strain rate but independent of environment. Lower ductility was exhibited for 310 SS at a strain rate of approximately 1×10^{-6} S^{-1} in inert atmospheres (He, Ar) as well as H_2S and H_2S/H_2O gases. The specimens tested previously in the inert atmospheres had some oxide on the surface even though the gas was passed through a liquid nitrogen trap to remove water vapor. The oxide also could have been formed from the low concentration (1.5 to 5 ppm) of oxygen in the gas. Several more 310 SS specimens were tested in inert atmospheres using an inert gas purifier to remove oxygen. Liquid nitrogen cold traps were also used to remove the water vapor. Fig. 1 is the stress-strain curve for a 310 SS specimen tested at 1000°F at the slow strain rate of $8.43 \cdot 10^{-7}$ S^{-1} in a helium atmosphere using the inert gas purifier. The fracture of this specimen was brittle with the accompanying low ductility and secondary cracking. A light gray oxide was still present on the surface of the specimen. Fig. 2 is a stress-strain curve of a 310 SS specimen tested in argon using the inert gas purifier at a slow strain rate of $8.4 \cdot 10^{-7}$ S^{-1} at 1000°F. The fracture was also brittle with the accompanying low ductility and secondary cracking. A light gray oxide was still present on the surface of the specimen. Another 310 SS specimen was tested in ultra-pure helium at a static pressure (no flow) with liquid nitrogren cold traps at both the entrance and exit to the test cell. Fig. 3 is the stress-strain curve for this specimen which again illustrates the brittle fracture and low ductility at the slow strain rate of $8.4 \cdot 10^{-7}$ S^{-1} at 1000°F. A light gray oxide was again present on the surface of the specimen. To date we have been unable to obtain a tested specimen that was free of any surface oxide when using various inert atmospheres. Another 310 SS specimen was tested this time in vacuum. The vacuum was attained by the in-house vacuum line (726 mm Hg). Fig. 4 is the stress-strain curve for this specimen tested at $8.4 \cdot 10^{-7}$ S^{-1} at 1000°F. Again the fracture was brittle with low ductility and secondary cracking. A light blue oxide was present on the surface of the tested specimen. Because of the color, the oxide appears to be thinner than the ones obtained from the inert atmospheres.

Since we have been unable to obtain an oxide free specimen when tested in an inert atmosphere or vacuum, we proceeded to test 310 SS at different strain rates and temperature assuming that the oxide on the surface of the specimens was not part of the mechanism that produced brittle fracture. Fig. 5 is a stress-strain curve of a 310 SS specimen that was tested at a faster strain rate of $1.3 \cdot 10^{-4}$ S^{-1} at 1000°F in a helium atmosphere where the gas was passed through the inert gas purifier and a liquid nitrogen trap. The fracture was ductile with no secondary cracking. The stress-strain curves in Fig. 6 show the effect of strain rate on two 310 SS specimens tested at 1000°F in dry helium. These curves could also be interpreted as the effect of time at

temperature on the properties of stress and strain. The embrittlement phenomenon seen when testing at the low strain rate in either inert atmosphere or H_2S is believed to be due to strain induced diffusion of interstitial impurities to grain-boundaries causing a brittle phase to form. Sensitization (formation of chromium carbide in the grain boundary thereby leaving a chromium depleted region) is known to occur in 310 SS in the temperature range from 800 to 1650°F. With this in mind, a 310 SS specimen was tested at 700°F at a slow strain rate of $8.43 \cdot 10^{-7}$ S^{-1} in dry helium using the gas purifier. The stress-strain curve for this specimen is shown in Fig. 7. The fracture was ductile with no secondary cracking. Fig. 8 shows the effect of temperature on the stress-strain curves of 310 SS when tested at a slow strain rate of $8.43 \cdot 10^{-7}$ S^{-1} in a dry helium atmosphere. The curves do seem to show evidence of embrittlement within the temperature range at which sensitization occurs, however, when tested below this range the material remains ductile. The results of a compositional analysis of the 310 SS were as follows:

Carbon	0.08%
Manganese	1.76
Phosphorus	0.027
Sulfur	0.021
Silicon	0.48
Nickel	19.66
Chromium	24.83
Molybdenum	.10
Copper	.17
Iron	Bal.

With the amount of carbon present, chromium carbide could readily be formed at the test temperature of 1000°F. The carbide forms very slowly only when the carbon content is on the order of 0.03% or less [1].

Other evidence that sensitization is occurring at the 1000°F test temperature and not at 700°F is shown in Figs. 9 and 10. Figs. 9A and B are photomicrographs of a 310 SS specimen as received and after testing at 1000°F at the slow strain rate of $8.43 \cdot 10^{-7}$ S^{-1} (brittle fracture), respectively. Fig. 9A shows the grain boundaries to be partially etched indicating some sensitization or carbide precipitation. Fig. 9B shows that the grain boundaries are completely etched indicating that further sensitization has occurred during testing. Figs. 10A and B are photomicrographs of a 310 SS specimen as received and after testing at 700°F at the slow strain rate of $8.43 \cdot 10^{-7}$ S^{-1} (ductile fracture), respectively. Fig. 10A shows the grain boundaries to be partially etched indicating some sensitization or carbide precipitation. Fig. 10B shows that the grain boundaries are not more deeply etched than in Fig. 10A indicating little or no further sensitization or precipitation occurred while testing at 700°F. (The same etching time was used for all specimens).

The brittle fracture which could be caused by the carbide precipitation only occurs at very slow strain rates. This point was made in an earlier report when a 310 SS specimen was held at 1000°F for 72 hours under a no load condition and then tested at a fast strain rate at 1000°F. The result was a ductile fracture with 34% elongation. If the temperature or time at temperature causes the sensitization which in turn causes the embrittlement, then the above test would have shown a brittle fracture. The result shows that a necessary condition for brittle fracture is a slow strain rate at temperature indicating

either a complicated mechanism or more than one mechanism of brittle failure.

A literature search was started on some work done in the 1950's and early 1960's regarding the strain rate dependent embrittlement of austenitic alloys. The literature search has shown that there may be several mechanisms that cause the brittle failure. Phase transformation in the alloy could be occurring when it is being plastically deformed during testing. Slow strain rate embrittlement or strain aging embrittlement (a facet of slow strain rate embrittlement) could be a mechanism for failure. The straining and aging occurs during the test when the strain rate and temperature are appropriate to allow sufficient mobility to a particular interstitial element involved. The migration of the interstitial element to grain boundaries, for example, can cause a brittle phase to form. Some of the interstitial alloying elements which have an influence on the mechanical behavior of alloys are carbon, nitrogen, oxygen, and boron. Of the literature searched, all the authors [2, 3, 4, 5] agree that the delayed brittle failure can only be detected by slow strain rate tests.

Plans: Test 347 and 310 S stainless steel and compare data with the 310 stainless steel data. The stabilized 347 SS is recommended for service where intermittent heating and cooling occurs between 800 and 1650°F to avoid intergranular embrittlement, whereas, the 310 stainless steel is recommended for service at constant elevated temperatures. The 310 S stainless steel which is low in carbon to reduce the precipitation of intergranular carbides can be used in the 800 to 1650°F zone for several hours but is not satisfactory for long-time service in the sensitizing temperature range because it is not completely immune to the formation of carbides which are detrimental to the corrosion resistance of the alloy. The literature search for data regarding strain-rate dependent embrittlement of austenitic alloys will continue.

Highlights: Early in the year, smooth round brass specimens were tested in water vapor saturated ammonia and were found to be susceptible to stress corrosion cracking in the gaseous atmosphere at a strain rate that was roughly within an order of magnitude of what was observed for brass in an aqueous medium. It was found that elongation at failure and reduction in area were better indicators of susceptibility to stress corrosion cracking than ultimate tensile strength. The ultimate tensile strength depended on the state of the specimen, that is, whether it was cold worked or annealed. The pre-condition of the specimen had less of an affect on elongation and reduction in area. The furnaces and their associated power supplies and controllers were calibrated after much delay due to manufacture's errors in the operating manuals (which were corrected by us in cooperation with Leeds and Northrup Co.).

Stainless steel Type 310 was picked as a starting material for testing in the constant strain rate machines because of its excellent resistance both to corrosion and oxidation at high temperatures and because of its high strength at elevated temperatures, thus making it a very desirable steel for elevated temperature service. The 310 SS was first tested in an H_2O/H_2S gaseous mixture at 1000°F. Some of the early data indicated that SCC was occurring at slow strain rates in the H_2O/H_2S environment. The same was

noted for 310 SS in a H_2S environment in the absence of water vapor at the slow strain rate. As we subsequently found, the 310 SS also failed by brittle fracture with low ductility in a helium environment at 1000°F at slow strain rates. It was then realized that what was earlier thought to be SCC was probably failure due to sensitization (precipitation of carbides or nitrides in the grain boundaries).

A visit was made to the low BTU coal gasification pilot plant at Morgantown, West Virginia to discuss the possibility of insertion of SCC specimens in their plant.

Three talks have been given by Mr. Ugiansky concerning the constant strain rate testing technique at the ASM/AIME Symposium on "Materials Behavior in Coal Gasification Environments", at the NACE, Corrosion/76, Corrosion Research Conference, and at the MFPG Symposium on "Prevention of Failures in Coal Conversion Systems".

References

1. Heat Treating of Stainless Steel, Source Book on Stainless Steels, ASM, pp. 162-173 (1976).

2. Uhlig, H. H. and White, R. A., Some Metallurgical Factors Affecting Stress Corrosion Cracking of Austenitic Stainless Steels, Trans. ASM, Vol. 52, pp. 830-846 (1960).

3. Troiano, A. R., The Role of Hydrogen and Other Interstitials in the Mechanical Behavior of Metals, Trans. ASM, Vol. 52, pp. 54-80 (1960).

4. Hsiao, C. M. and Dulis, E. J., Effect of Interstitial Carbon Plus Nitrogen and Precipitation Reactions on the Properties of Austenitic Cr-Mn-C-N Steels, Trans. ASM, Vo. 52, pp. 855-877 (1960).

5. Shepherd, O. C. and Schalliol, W., The Effect of Environment on the Stress-Rupture Properties of Metals at Elevated Temperatures, Symposium on Corrosion of Materials at Elevated Temperatures, ASTM, Special Tech. Publ. No. 108, pp. 34-41 (Apr. 1951).

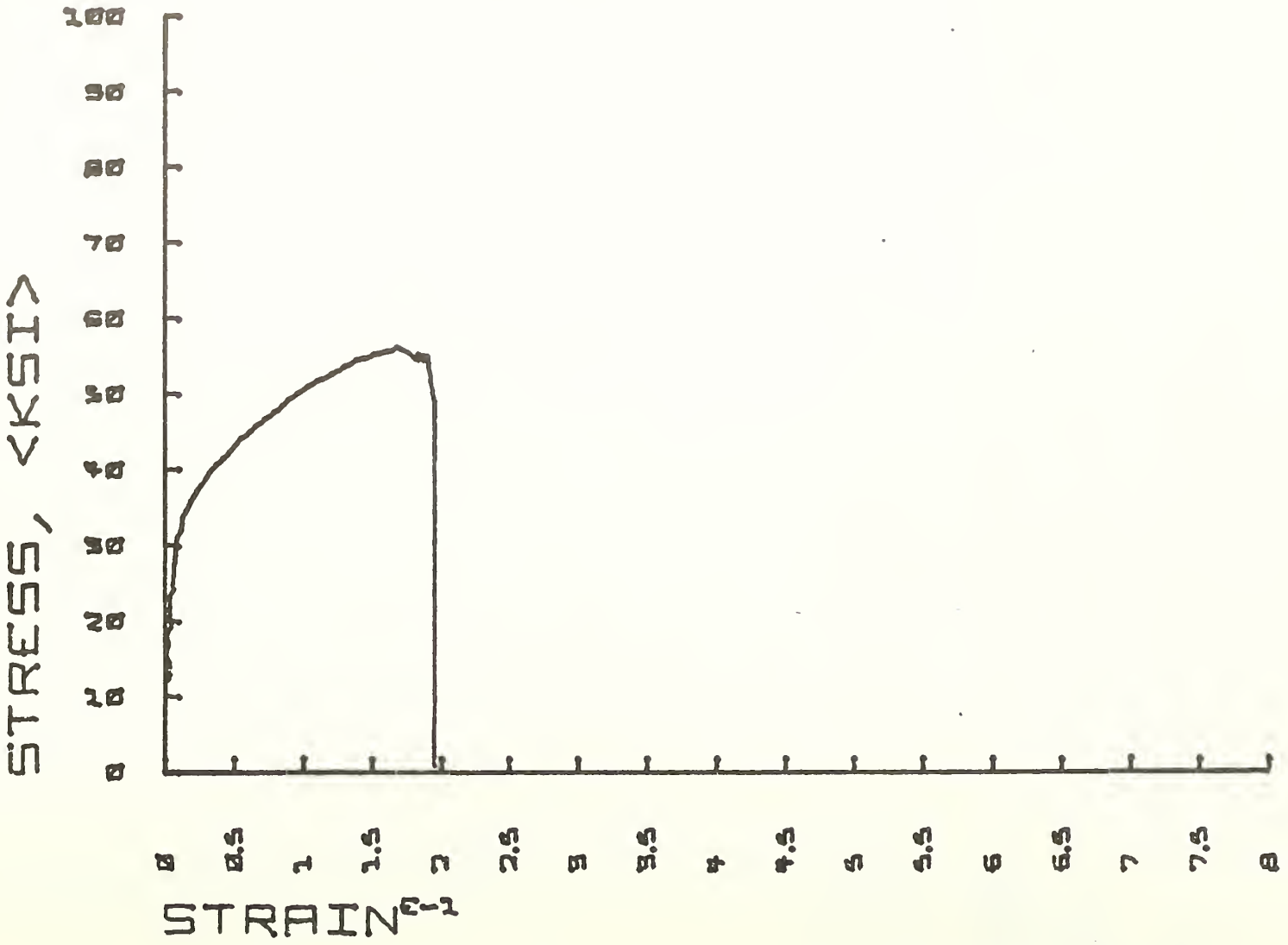

Fig. 1. Stress-strain curve for 310 SS in dry helium (passed through an inert gas purifier) at a constant strain rate of $8.43 \cdot 10^{-7}$ S^{-1} at 1000°F.

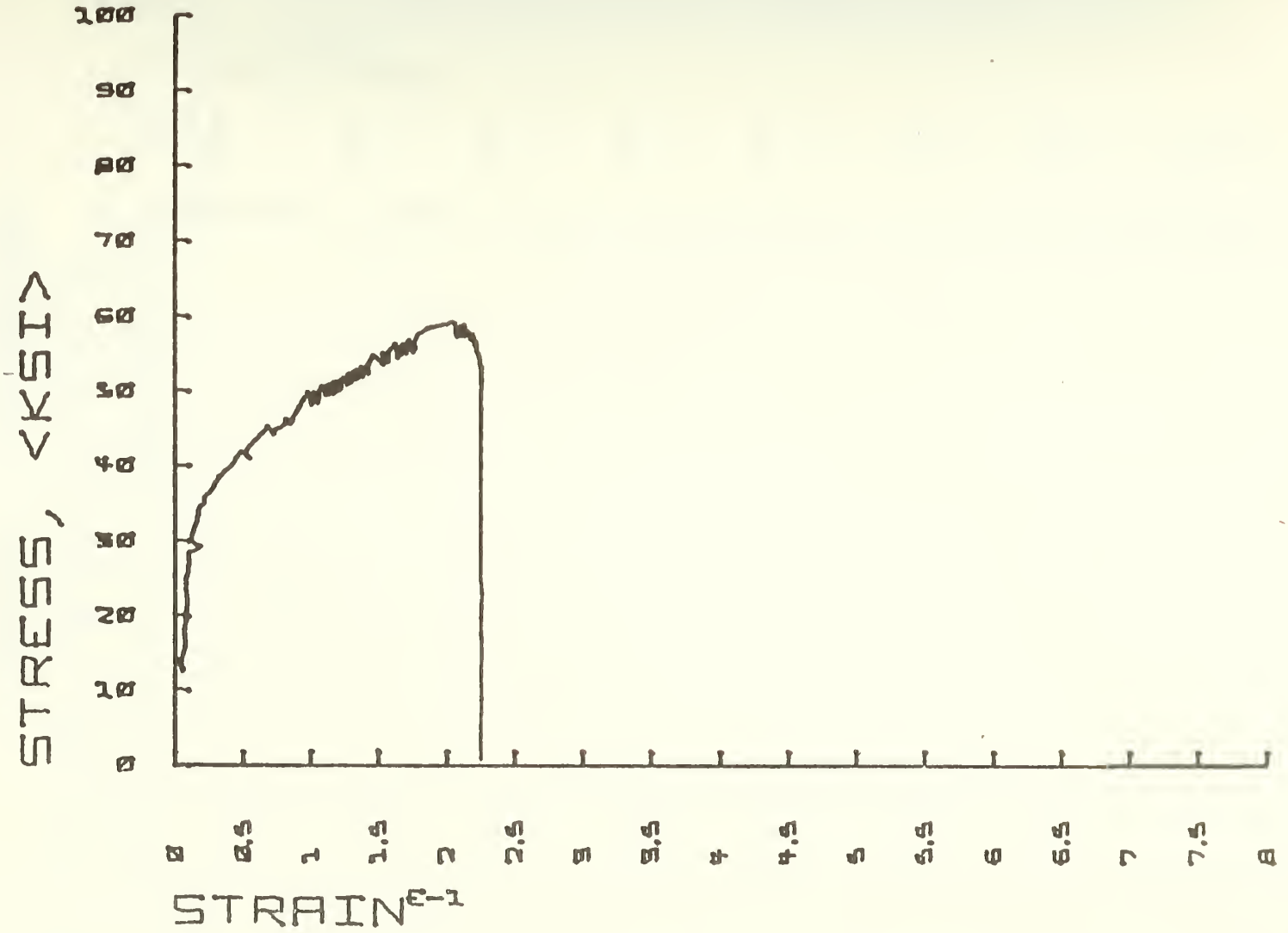

Fig. 2. Stress-strain curve for 310 SS in argon (passed through an inert gas purifier) at a constant strain rate of $1.06 \cdot 10^{-6}$ S^{-1} at 1000°F.

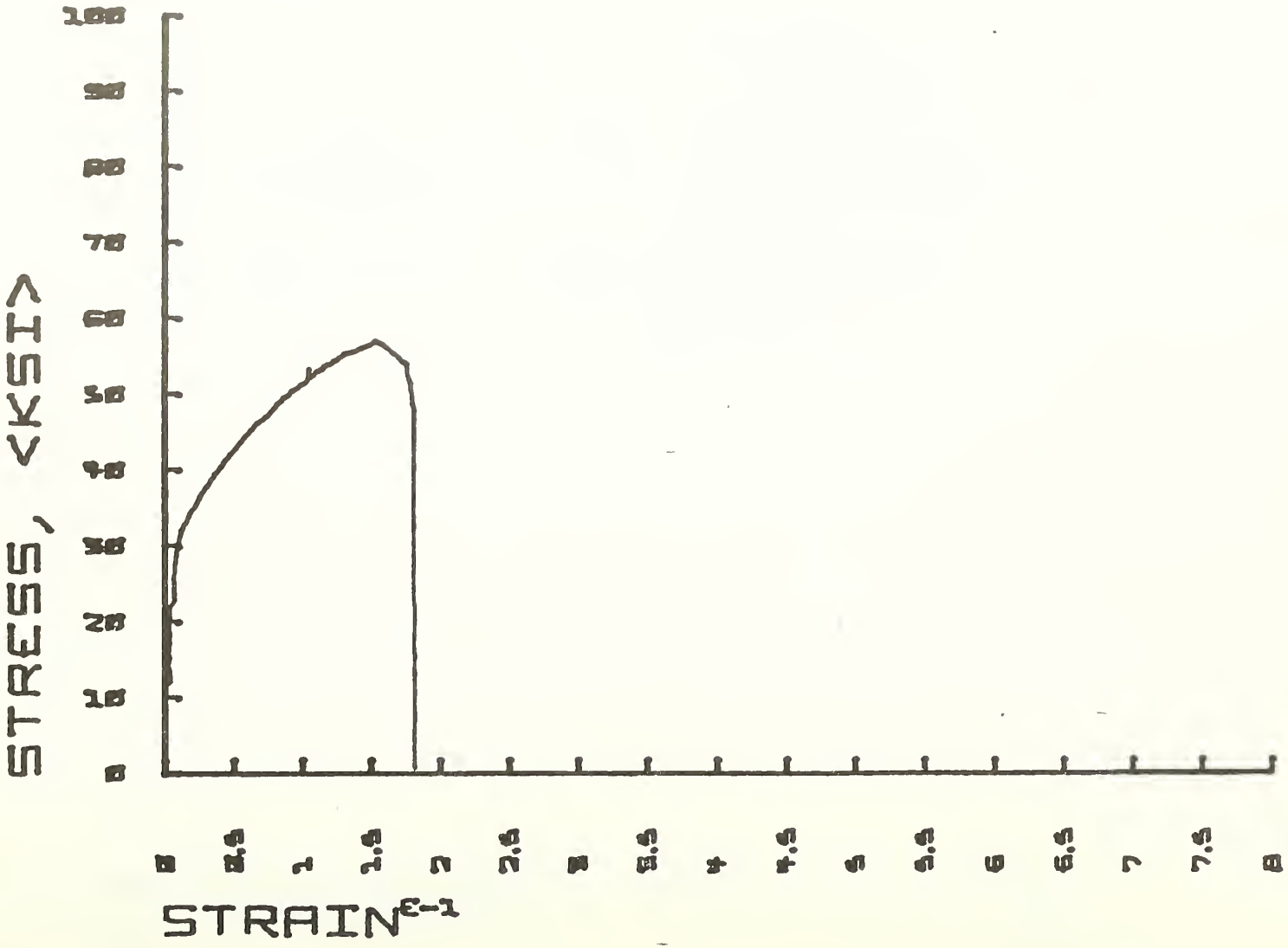

Fig. 3. Stress-strain curve for 310 SS in ultra-pure helium at a constant strain rate of $8.43 \cdot 10^{-7}$ S^{-1} at 1000°F.

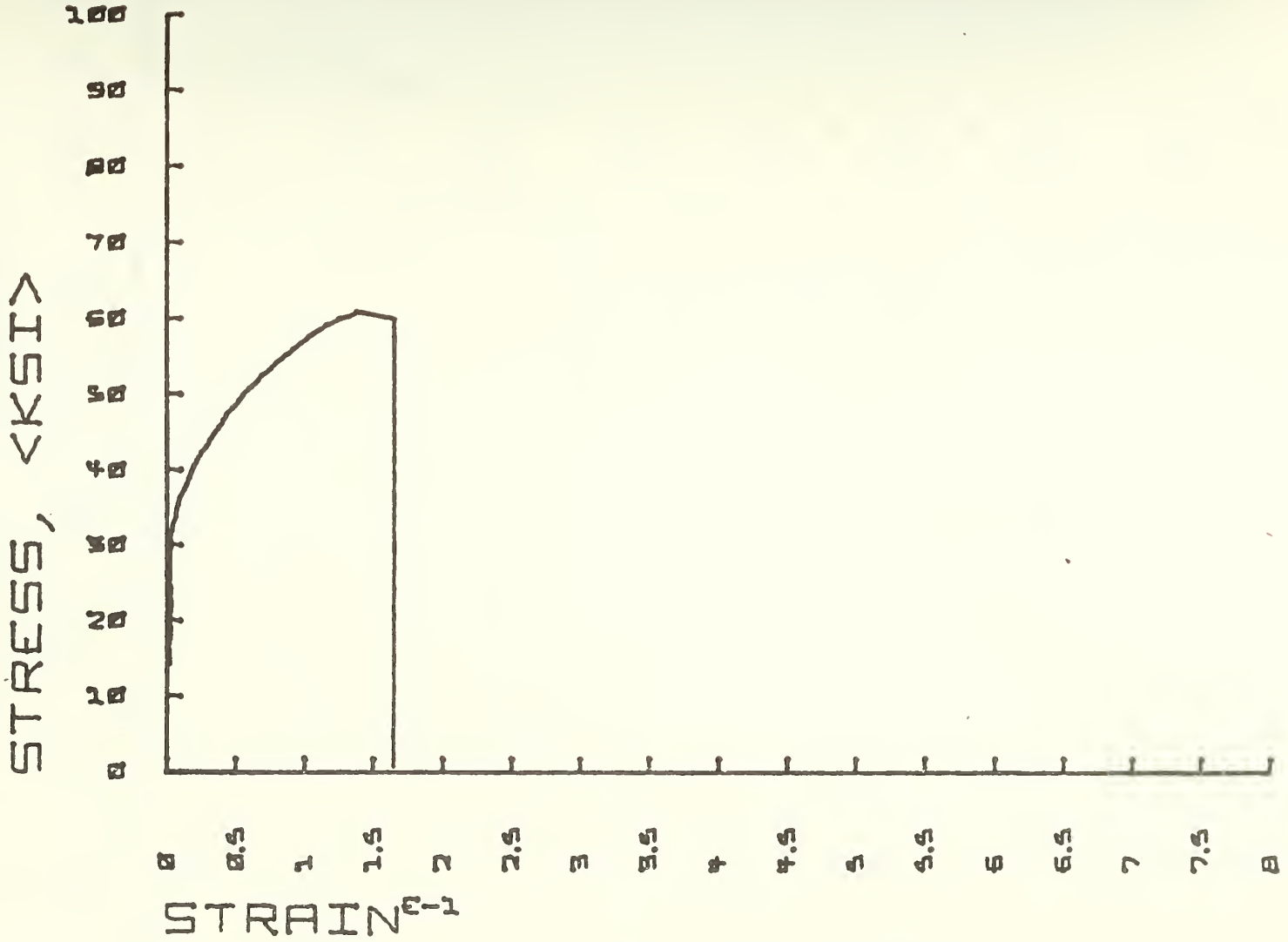

Fig. 4. Stress-strain curve for 310 SS in vacuum (in-house vacuum line, 726 mm Hg) at a constant strain rate of $8.43 \cdot 10\text{-}7\ S^{-1}$ at 1000°F.

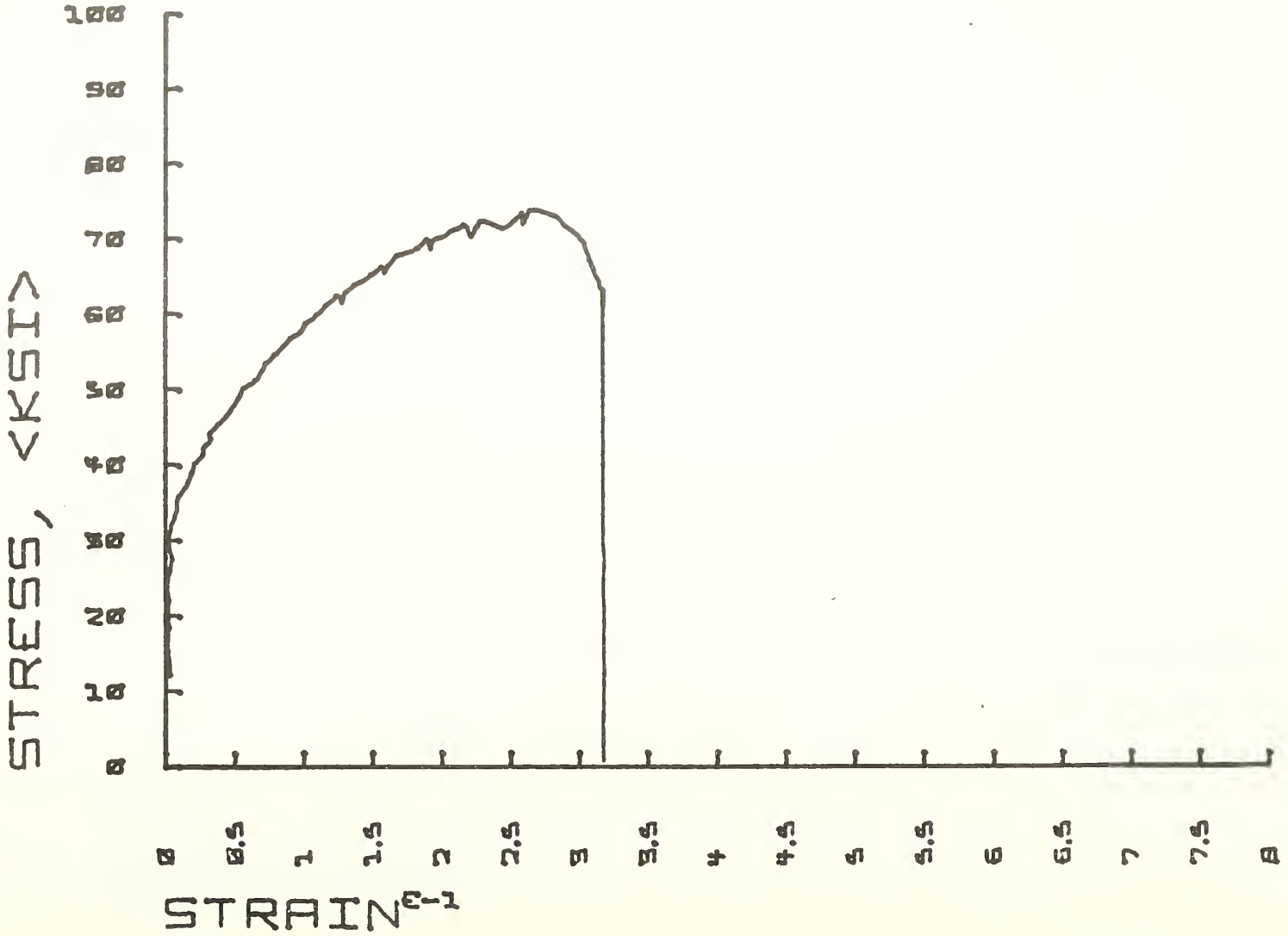

Fig. 5. Stress-strain curve for 310 SS in dry helium (passed through inert gas purifier) at a constant strain rate of $1.30 \cdot 10^{-4}$ S^{-1} at 1000°F.

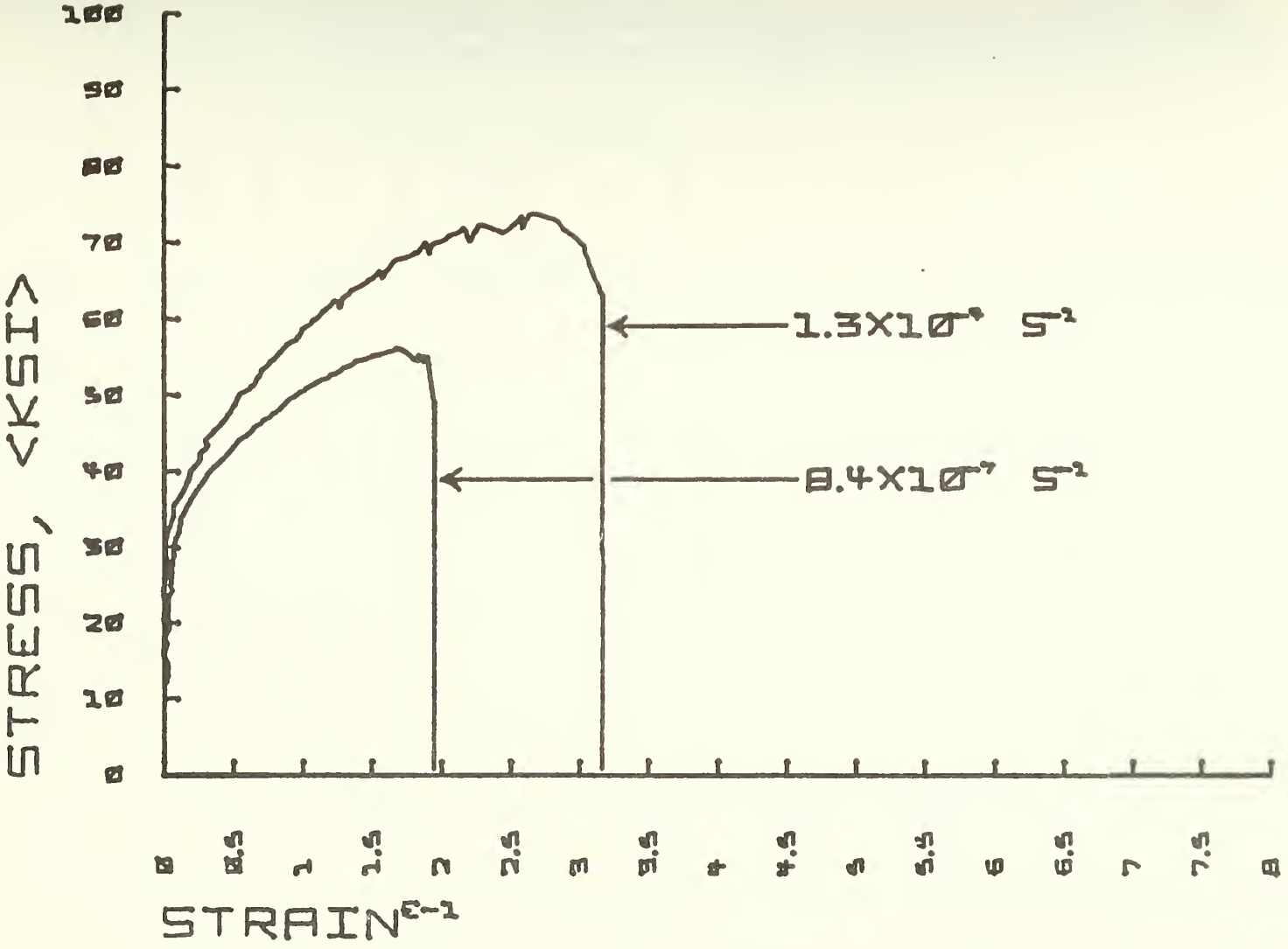

Fig. 6. Stress-strain curves for 310 SS showing the effect of strain rate when tested in dry helium (passed through an inert gas purifier) at 1000°F.

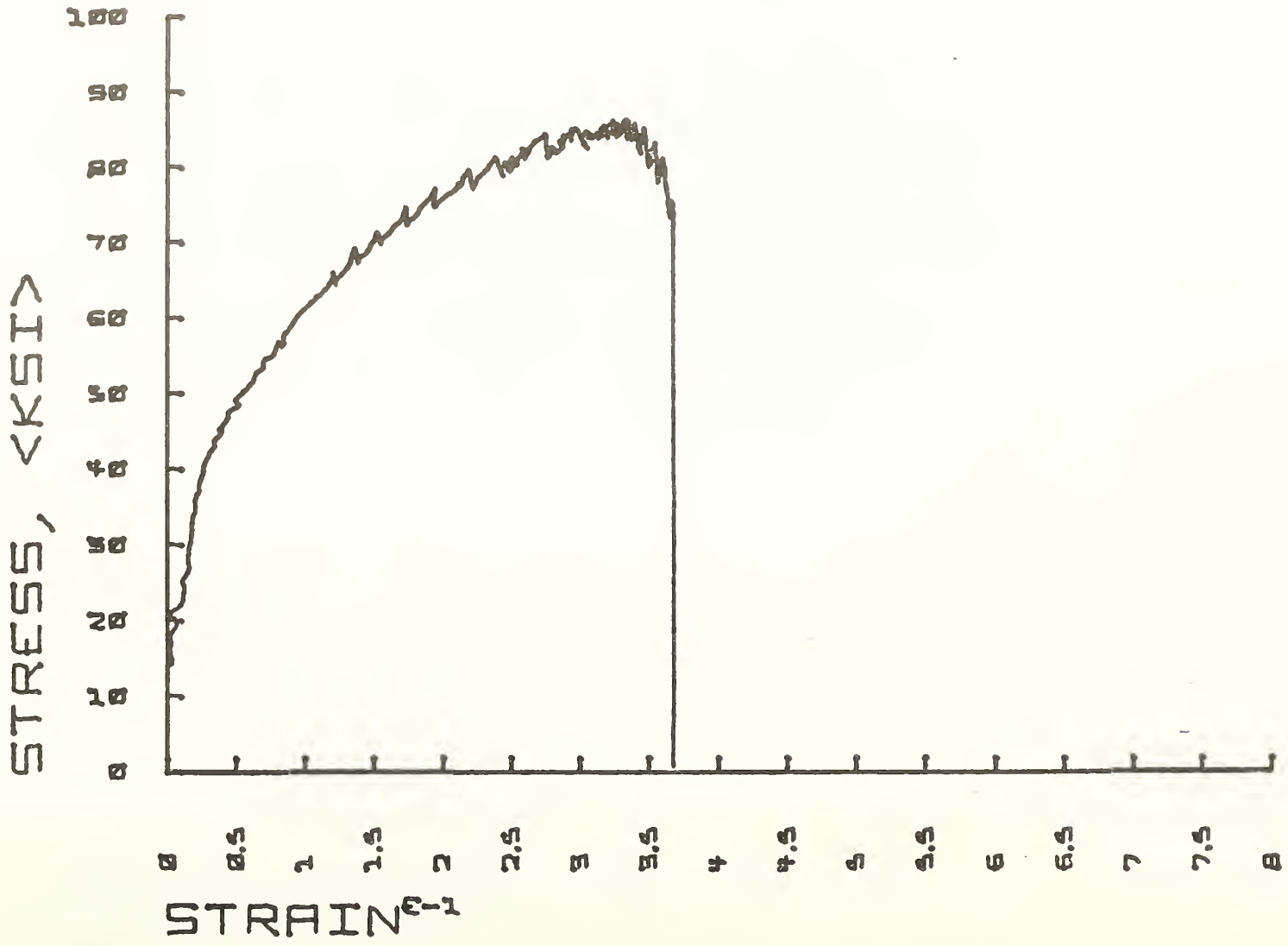

Fig. 7. Stress-strain curve for 310 SS in dry helium (passed through inert gas purifier) at a constant strain rate of $8.43 \cdot 10^{-7}$ S^{-1} at 700°F.

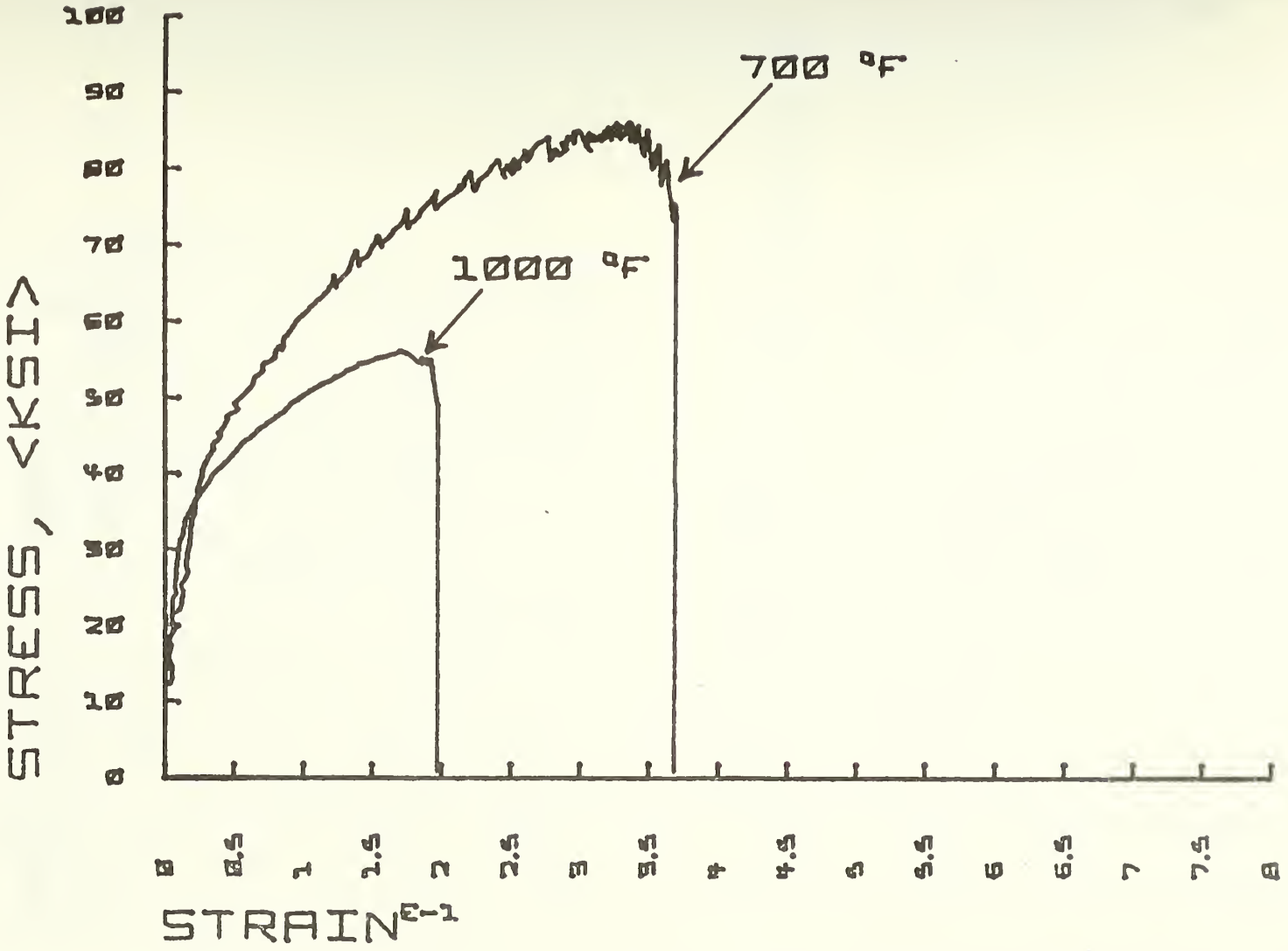

Fig. 8. Stress-strain curves for 310 SS showing the effect of temperature when tested in dry helium (passed through inert gas purifier) at a constant strain rate of $8.43 \cdot 10^{-7}$ S^{-1}.

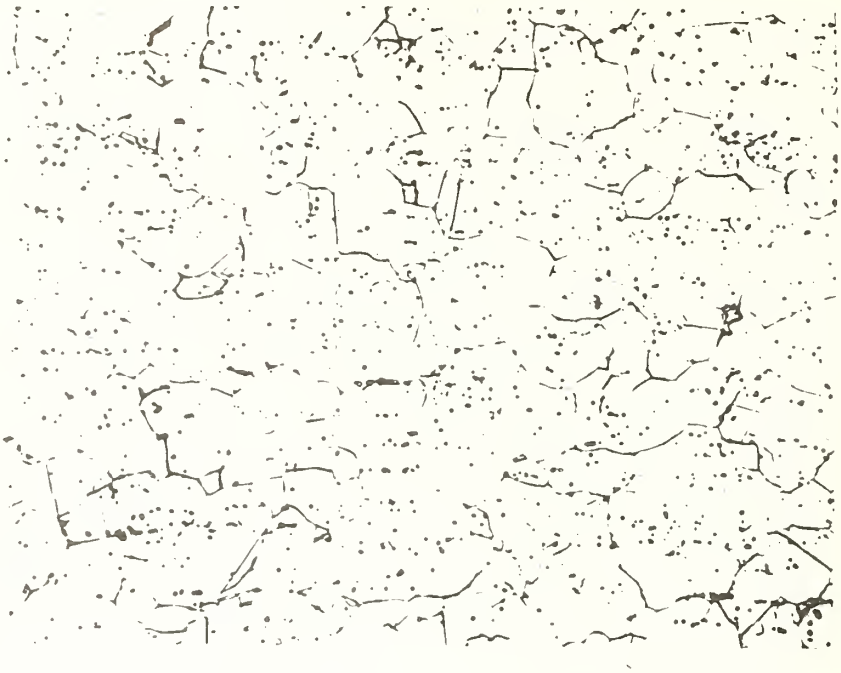

Fig. 9A. Photomicrograph of 310 SS as received. Etched for 5 seconds at 5 volts in 10% oxalic acid. 500 X

Fig. 9B. Photomicrograph of 310 SS after testing at 1000°F at a constant strain rate of $8.43 \cdot 10^{-7}$ S^{-1}. Etched for 5 seconds at 5 volts in 10% oxalic acid. 500 X

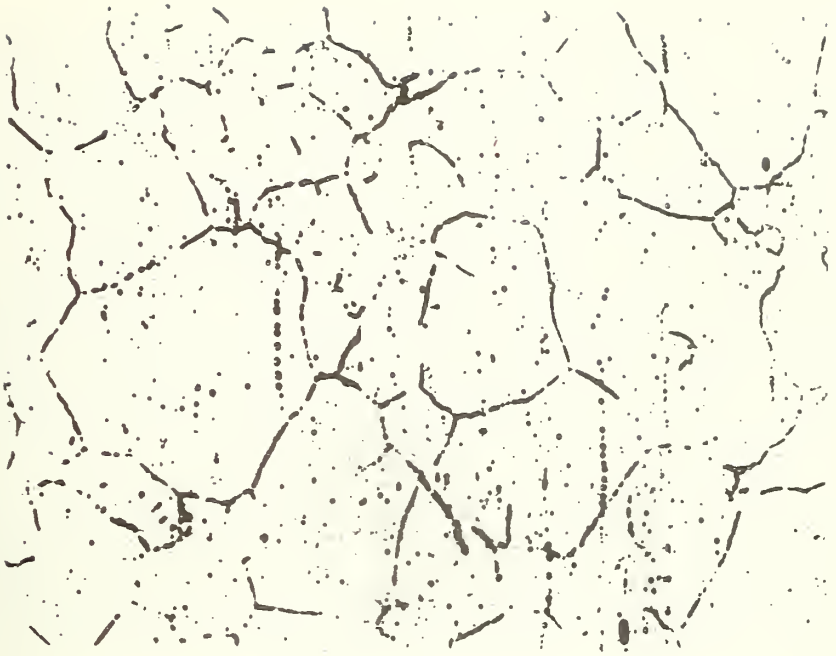

Fig. 10A. Photomicrograph of 310 SS as received. Etched for 5 seconds at 5 volts in 10% oxalic acid. 500 X

Fig. 10B. Photomicrograph of 310 SS after testing at 700°F at a constant strain rate of $8.43 \cdot 10^{-7}\ S^{-1}$. Etched for 5 seconds at 5 volts in 10% oxalic acid. 500 X

b) Erosive Wear (A. W. Ruff, L. K. Ives, J. P. Young, 312.03, April - June 1976)

Progress: At this time tests conducted in the flame - erosion apparatus have produced a fairly complete set of data covering the erosion of 310 ss in the velocity range 10 - 70 m/s using 100 mesh (150 μm) SiC abrasive materials. These experiments were restricted to normal (90°) incidence and were carried out both at 975°C in combustion gas atmospheres and at 25°C in air. A paper entitled "Erosion in 310 Stainless Steel at 975°C in Combustion Gas Atmospheres" describing most of these results was prepared and has been accepted for presentation at the November 1976 ASME meeting in New York City and for publication in the J. of ASME. A second paper describing some of the work was also presented at the April MFPG meeting in Columbus, Ohio and is attached to this report. Together the papers summarize the significant results that have been described in previous quarterly reports with some significant additional information obtained in the current quarter. A summary of the erosion data on 310 ss is given in Fig. 1 where the log of erosion (sample weight loss in mg/ weight of abrasive in g) is plotted against the log of the particle velocity. A similar graph was presented in the last quarterly report (January - March 76). However, there an additional curve at 975°C was included showing the erosion vs velocity dependence for SiC abrasive material that contained impurities which resulted in the adherence of abrasive particles to the sample surface at low velocities. The present graph includes only data obtained with non-adhering SiC abrasive material. In addition, redetermination of the characteristic particle velocity calibration curves of the erosion appartus has led to some changes with respect to the earlier figure.

An important aspect of the elevated temperature studies has concerned an investigation of the morphology and composition of the eroded-corroded surfaces. These investigations were carried out in a scanning electron microscope equipped with an energy dispersive x-ray analysis system. The specimens were subsequently sectioned normal to the eroded surfaces to obtain information on the thickness, structure and in depth composition of the oxide scale. A sample exposed at 975°C with a particle velocity of 14 m/s is shown in Fig. 2.

A brief summary of results - most of which are contained in the above mentioned papers-is as follows. Considerable variations of oxygen - propane gas ratio with associated changes in combustion gas composition at the specimen location have little effect on erosion rate. At 975°C the erosion rate is approximately proportioned to the velocity raised to the 1.8 power while at 25°C in air the velocity exponent is approximately 2.5. At 15 m/s the erosion rate is about an order of magnitude greater at 975°C than at 25°C. However, as a result of the different velocity exponents, the erosion rates appear to converge at higher velocities. Over the velocity range studied, 10 - 70 m/s at 975°C with a flux of 0.04 g/cm^2 a relatively thick oxide layer exists on the eroded surfaces. At the low velocity end of the range, erosion was confined entirely to the oxide layer while at the higher velocities particles were able to penetrate the oxide layer causing direct damage to the underlying metal. The morphology of particle indentations suggested a ductile flow of the oxide layer at 975°C.

A new series of tests was begun with the purpose of measuring the angular dependence of erosion at 975°C. However, in preparation to conducting these tests some modifications were made in the flame-erosion appartus. The most significant concerned the use of tungsten-carbide (WC) nozzles in place of the rapidly wearing stainless steel nozzles. It has been necessary to replace the stainless steel nozzles after each test (∿ 400 g of abrasive) at low velocities and after 200 g of abrasive had passed through the nozzle at high velocities (∿ 40 m/s at 25°C and ∿ 70 m/s at 975°C). Although precise data have not yet been obtained, the life of the WC nozzles is substantially greater than that of the stainless steel nozzles. The slightly smaller inside diameter (1.54 mm vs 1.59 mm) of the WC nozzles has required the redetermination of the particle velocity vs air flow curves.

Some preliminary measurements of angular dependence have been carried out at a particle velocity of 34 m/s. Initially, simple wedge shaped samples were used. However, it was found that the geometry led to a substantial temperature gradient over the sample face. As much as 70°C was obtained over a distance of 1.3 cm, the length of the exposed face, at a wedge angle of 20°. Temperature measurements were conducted with an optical pyrometer focussed on the sample surface. A thermal shield of cylindrical shape was constructed to surround the specimen but this led to a reduction of only about 20% in the temperature gradient. A more substantial improvement was obtained by employing samples of the geometry shown in Fig. 3. A strip of 310 ss, 0.6 mm thick was carefully fitted over the top of the specimen and clamped in place during exposure so that only the intended specimen face was exposed to erosion. With this design at an average temperature of 975°C, a difference of 25°C was measured between the top and bottom of the 1.3 cm long face.

A few 975°C tests were conducted at attack angles of 20°, 30°, and 40°. In all cases the erosion rate was signficantly less than at normal (90°) impingement. However, the erosion rate at 20° was larger than at 30° and 40°. This suggests the existance of an intermediate minimum in erosion between 20° and 90° followed by a low angle maximum between 0° and 20°.

Tests using the Roberts Abrader have been conducted for several purposes. A new tungsten carbide nozzle (0.5 mm inside diameter) was placed into operation and its performance was evaluated. A test was conducted at 25°C using 304 ss material with CO_2 propellent and 50 μm Al_2O_3, at flow rates of 5 to 18 grams/minute. The relative weight loss and the relative cavity depth formed at each flow rate was found to be reasonably independent of flow rate as shown below.

Abrasive Flow (g/min.)	Erosive Wear	
	Wt. Loss/Wt. Abr. (10^{-3})	Penetration/Wt. Abr. (μm/g)
5	0.17	6.6
8	0.19	7.1
12	0.17	6.7
15	0.19	8.3
18	0.19	8.6

This indicates that abrasive flow rates in this equipment is not critical over the usual range employed.

Initial tests of the erosion resistance of thick chromium plate on steel gave substantially larger wear resistances than those obtained for the stainless steels and alloys containing nickel we have studied. A series of tests was conducted at various temperatures, angles of incidence and particle velocities. The abrasive used was 50 μm Al_2O_3 (90° incidence for velocity tests) with CO_2 propellent gas for 2 min. exposure. Chromium plate proved to have the largest erosion resistance in all the tests. Some of the data are shown below along with those of comparative alloys.

Specimen	Particle Velocity (m/s)	Particle Velocity Dependence of Relative Weight Loss (10^{-3}) at Indicated Temperatures			Angle (deg)	Angle of Attack Dependence of Relative Weight Loss (10^{-3}) at Indicated Temperatures and 31 m/s	
		25°C	500°C	1000°C		25°C	500°C
Cr Plate	11	0.07	0.06	0.62	20	0.15	0.01
	21	.11	.08	.61	30	.13	.02
	31	.15	.11	.46	45	.15	.08
	42	.14	.20	.73	70	.14	----
	52	.16	.18	----	90	.17	.11
310 ss	11	0.08	0.09	----	20	----	0.47
	21	.15	.20	----	30	----	.28
	31	.18	.25	----	45	----	.30
	42	.21	.33	----	70	----	.34
	52	.29	.55	----	90	----	.14
304 ss	11	0.10	0.10	----	20	----	0.33
	21	.19	.21	----	30	----	.35
	31	.24	.30	----	45	----	.26
	42	.25	.38	----	70	----	.23
	52	.33	.29	----	90	----	.26

The angle of attack dependence of erosion at 500°C is shown in Fig. 4 for several alloy in comparison to the chromium plate on steel. The low angle peak loss is not found for the Cr plate, however, a gradual increase in erosion with increasing angle is seen.

Three different types of chromium were compared for erosion resistance in the Jet Abrader at 25 and 500°C. Rolled, ductile, ultra-pure chromium and a chromium-low iron alloy were compared with thick chromium plate on steel. The abrasive used was 50 μm Al_2O_3 at 31 m/s velocity, nozzle at 45° and 1 cm from the specimen. Average loss of three tests for each type and temperature are shown below.

Unit	Temp (°C)	Cr Plate	Pure Cr	Cr-Fe
$\frac{\text{Wt. Loss}}{\text{Wt. Abr.}}$ (mg/g)	25	0.13	0.14	0.26
	500	0.05	0.11	0.21
$\frac{\text{Penetration}}{\text{Wt. Abr.}}$ (μm/g)	25	3.8	8.9	6.6
	500	4.9	7.5	5.5
Hardness (KHN_{200})	25	985	230	587

The exact composition of the Cr-Fe alloy is not yet known but appears to be a few percent of iron. The pure chromium and the Cr-Fe alloy were prepared by the Bureau of Mines several years ago.

The experimental Haynes 8077 alloy (16Cr, 4Al + Ni + Y_2O_3) has been tested in the Roberts unit at 500°C. Al_2O_3 (50μm) abrasive was used at 31 m/s velocity with the nozzle at 45° angle and 1 cm from the specimen. Test time was 2 minutes. The propellent gas was CO_2. The results were compared with those of several alloys previously tested as shown below using the same conditions.

Unit	Alloy Type								
	250MS	304	310	316	446	601	671	800	8077
Mean Wt. Loss (mg)	9.9	2.3	2.1	2.2	2.1	2.0	1.6	2.8	4.0
Mean Penetration (μm)	167	130	138	157	114	150	137	187	171
$\frac{\text{Wt. Loss}}{\text{Wt. Abr.}}$ (mg/g)	0.95	0.23	0.20	0.21	0.20	0.19	0.15	0.27	0.38
$\frac{\text{Penetration}}{\text{Wt. Abr.}}$ (μm/g)	16.1	12.5	13.3	15.1	11.0	14.4	13.2	18.0	16.4

The wear resistance of the 8077 alloy appears to be somewhat lower then that of most of the other alloys at 500°C under these conditions.

Development continues on the electronic control unit to remove abrasive flux variations during erosion test exposure. This feedback control device senses the exit gas pressure at the nozzle and uses any variation to adjust the vibrator drive amplitude on the abrasive chamber. The unit is in operation at this time and adjustable parameters are being optimized.

Plans: The effect of sulfur contamination will be studied. Characterization of scale deposits will be conducted. Measurements on the alloys of interest will continue. The electronic flow control unit will be further developed.

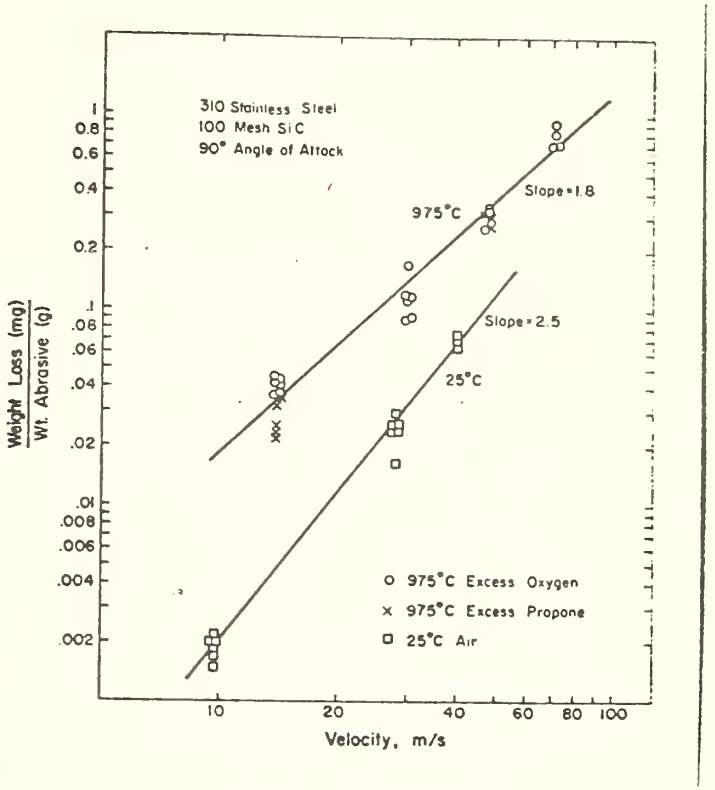

Fig. 1 Velocity dependence of erosion at 975°C and 25°C.

Fig. 2 Cross-section of surface after exposure to erosion at 975°C to a particle velocity of 14 m/s.

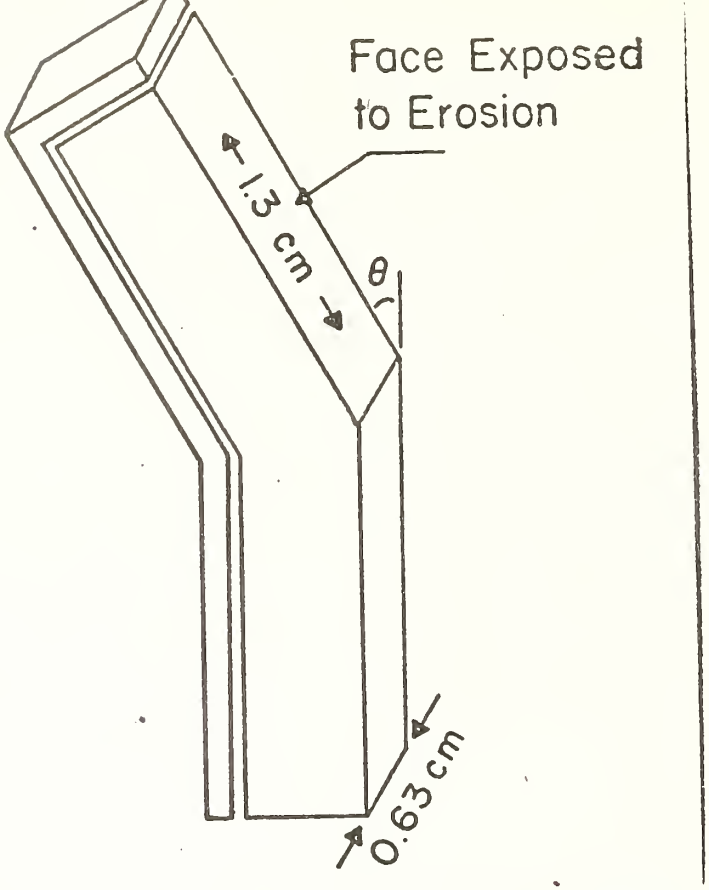

Fig. 3 Erosion test specimen design for angular dependence measurements

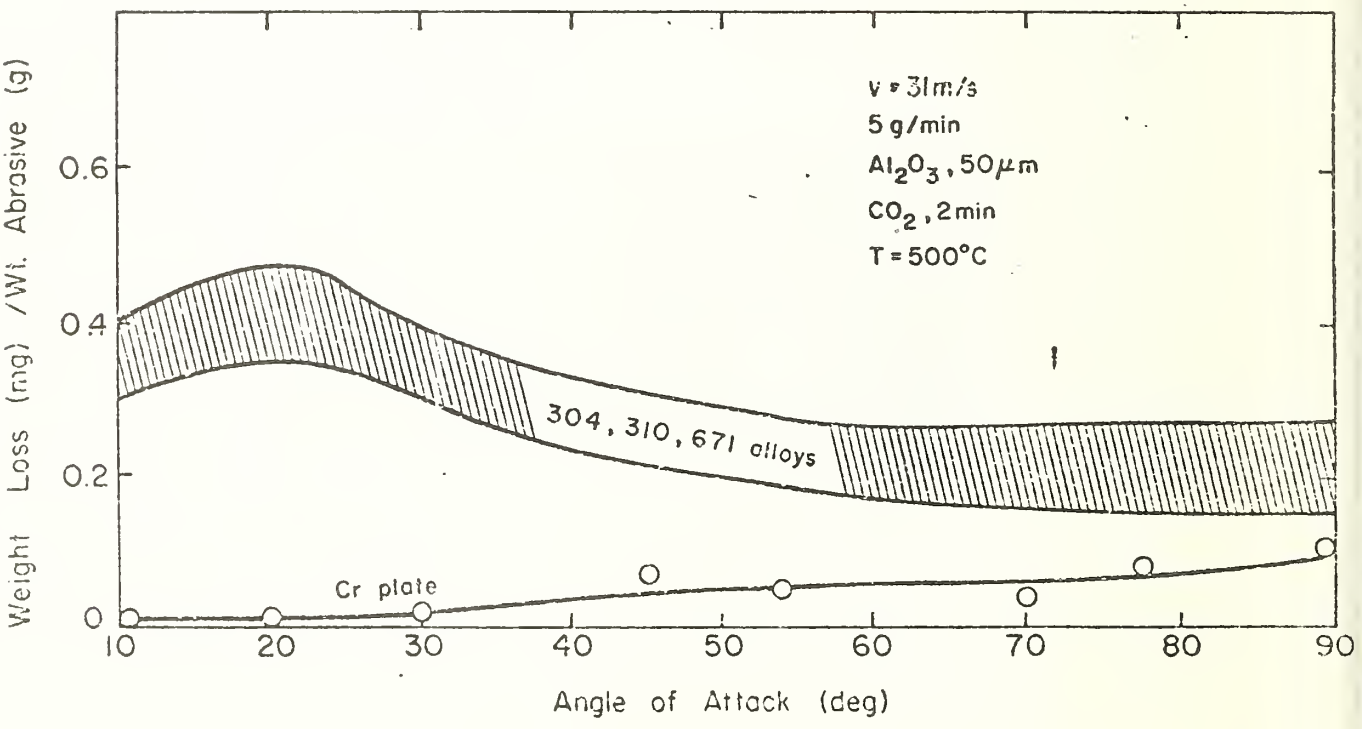

Fig. 4 Angle dependence of erosion at 500°C for indicated alloys and chromium plate on steel

Proceedings of the Mechanical Failures Prevention Group
Columbus, Ohio (April 1976)

PARTICLE EROSION MEASUREMENTS ON METALS AT ELEVATED TEMPERATURES

L. K. Ives, J. P. Young, and A. W. Ruff
National Bureau of Standards
Washington, D.C. 20234

Abstract: Measurements of the erosive wear of metals resulting from impact by abrasive particles under reactive environmental conditions are being conducted. Specimens of several stainless steel and nickel alloys have been exposed to a gas stream containing abrasive particles. The particle flux, angle of attack, particle velocity, particle size, surface temperature and other significant variables were controlled. Different types of abrasives were used including Al_2O_3, SiO_2, SiC and pumice. Two different erosion test apparatus have been developed and used to obtain particle velocities from 10 to 90 m/s and temperatures up to 1000°C. Different gaseous atmospheres have been established during the erosion exposures. Weight loss measurements and penetration depth measurements were conducted on the specimens after exposure. Multiple alloy specimen packages were used in some experiments to obtain relative erosion data. Erosion rates were determined in the temperature range of 25 to 1000°C. Erosion depended on particle velocity over the range V^2 to V^3, increased with particle size, increased with particle hardness, and was maximum for an angle of attack around 20°. The effects of temperature and environment vary in a complicated way among the different alloys.

Key words: Abrasive particles, Erosion, Erosive wear, Metals, Oxidation, Wear.

Introduction: Studies of metal wear by erosion under various conditions have been conducted [1-6] at room temperature and in a few cases at elevated temperatures [7,8]. Industrial applications, for example in the petrochemical industry and in new industries such as coal gasification [9], require data on metal erosion under conditions of high temperature and reactive environments. Much of that information still needs to be acquired. Erosion of metals at room temperature has been found to depend on particle velocity in the range v^2 to v^3 [1,2]. The angular dependence of erosion exhibits a peak at about 20° angle of attack [1,4] and the effects of different particle sizes have been investigated [2,5]. Erosion can either increase or decrease with increasing temperature [7,8] depending on the metal and the atmosphere. The mechanisms of erosion have been studied using single particle impact techniques [10]. The present paper describes recent erosion measurements conducted on metals at room and elevated temperatures up to 1000°C in different gaseous atmospheres.

Experimental: Two different erosion testing apparatus have been used in the present work. One system was based on an instrument developed previously at this laboratory [11]. That instrument had been used principally to determine the durability of coatings.* Considerable attention was paid during its development toward achieving reproducibility of operation. Modifications introduced in the current program have been designed to extend the operating capabilities to elevated temperatures while maintaining that reproducibility. A schematic diagram of the system is shown in Fig. 1. In order to obtain data at elevated temperatures, the metal specimens were heated directly by passage of a dc current through them during erosion testing. Current values up to 200 A at 10 V were used to reach an operating temperature of 500°C and above. The metal specimen size was typically 3 cm long x 1 cm wide x 0.5 mm thick. Battery clips (gold plated) were used to achieve electrical contact at each end of the specimen during heating. A thermocouple pressed in contact with the underside of the specimen was used to determine the test temperature. The propellent gas-particle mixture was also heated. After injection of abrasive particles, the mixture passed through an eight foot length of 1.6 mm inside diameter stainless steel tubing that was heated by the passage of up to 60 A ac current along its length. The gas-abrasive particle mixture was discharged through a right angle tungsten carbide nozzle, 0.5 mm inside diameter. The exit gas temperature was adjusted so that the specimen temperature did not change during the test although it may have been as low as 300°C at high flow rates when the specimen was maintained at 500°C. The propellent gas used in the tests reported here was 99.9% CO_2. The exposure time during each test was 2 minutes. Table 1 lists some of the characteristics of this test apparatus.

Table 1

Range of Operating Parameters for Roberts Erosion Unit

Gas:	CO_2,O_2,CO, mixtures
Particle sizes:	5 to 50 μm (0.5 mm nozzle) 5 to 150 μm (1.25 mm nozzle)
Gas Pressure:	20-70 psig (0.14 - 0.49 MPa)
Particle velocity:	10-60-m/s
Solids concentration:	0.5 to 3 g/l
Particle flux:	0.5 to 3 g/cm^2-s
Specimen temperature:	ambient to 500°C+

*Roberts Jet Abrader, Kameras Instruments. This instrument is identified only for the purpose of adequately specifying the experimental procedure used.

The second erosion system has been described previously [12] and permitted test temperatures of 1000°C to be achieved. Briefly, a propane-oxygen-air burner was used to direct a stream of hot combustion gases containing entrained abrasive particles down a 41cm tube to impact on the specimen. The stream was approximately 2 cm in diameter. By changing the oxygen and propane flows, the composition of the gases impinging on the specimen could be varied. When oxygen was supplied in excess of the amount needed for complete combustion, an atmosphere composed of N_2, O_2, CO_2 and H_2O was produced. When excess propane was introduced, CO, H_2 and hydrocarbons were obtained in addition to the above gases. Test times were usually 60 minutes. Table 2 describes the operating features of this unit.

Table 2

Range of Operating Parameters for High Temperature Erosion Unit

Gas: Combustion gases; air

Particles: Al_2O_3, SiC

Particle sizes: 50-200 μm

Particle velocity: 10-90 m/s

Solids concentration: 0.005 to 0.02 g/l

Particle flux: 0.04 g/cm^2-s

Specimen temperature: ambient to 1000°C

Table 3

Parameters of Abrasive Particles Used in Erosion Tests

Type	Size (μm)	Hardness (HK@25°C)
SiC	150	2500
Al_2O_3	5	2100
Al_2O_3	50	2100
SiO_2	5-50	820
F-Pumice	5-100	560
4F-Pumice	5-50	560

The abrasives used in the tests reported here are listed in Table 3. Room temperature hardness values are listed. The Al_2O_3 abrasives are metallographic polishing grade material having a narrow size distribution. A collection of the 5μm Al_2O_3 particles is shown in Fig. 2. The particles passed only once through the system and were then discarded. The particle velocity was measured using the rotating disk, time-of-

flight method [13]. Velocity measurements were conducted at the test temperatures.

Weight loss values were determined by direct weighing after exposure and cleaning. Microscopic inspection of the surface indicated whether particle adhesion to the specimen was significant. If so, attempts were made to mechanically remove the adherent particles by light brushing. Since scale formation occurred at elevated temperatures, it was difficult to remove all adherent abrasive and yet not affect surface scale. Dimensional measurements of erosion crater depth and of specimen thickness loss were made using microscopic or micrometer methods with a precision of the order of ±1 to 10 μm depending on surface roughness. Examination of the eroded surfaces was conducted using optical and scanning electron microscope (SEM) methods.

Results

Studies at 25°C and 500°C: Examples of isolated particle impacts are shown in Fig. 3 after a low flux exposure of an SAE 52100 steel specimen. The rim of each erosion crater consists of exposed material that has been deformed plastically and which is susceptible to removal on subsequent particle impacts. That material is also more susceptible to attack in a chemically reactive environment. Measurements have been conducted at room temperature using the modified Roberts unit with different abrasive particle velocities. Relative weight loss and penetration measurements on 304 stainless steel are shown in Fig. 4 for 90° (normal) incidence, using two sizes of Al_2O_3 particles. The erosion loss depends on the velocity raised to about the 2.8 power in these tests. In general, we find that erosion is proportional to velocity in the range of $v^{2.5}$ to v^3 at room temperature. A greater erosion loss is seen here for the larger particles, 50μm Al_2O_3. The comparison between weight loss and penetration distance is usually complicated by such factors as erosion beam geometry changes when the abrasive type and size are changed. It is preferable to use the same erosion measure when comparing different metals.

The relative weight loss as a function of angle of attack α, the angle between the specimen surface and the incident particle stream, has been determined for 304 stainless steel at both 25°C and 500°C. The particle flow and velocity were maintained constant as the specimens were exposed at different angles to the particle stream. At 25°C a peak erosion loss occurs at about 20° followed by a gradual decrease as the angle is increased up to 90°. The angle dependence of erosion at 500°C is different. The low angle peak occurs at about 10°, followed by a rapid decrease and then little change occurs in the range 40-70°. The loss appears to increase again as 90° impingement is approached. At 500°C oxidation is more rapid than at room temperature, hence, the incident abrasive particles experience a different surface condition. The increased relative loss at 90° may be connected with the known erosion characteristics of brittle materials where the peak loss occurs at

normal incidence. The oxide film or scale probably behaves in a more brittle manner than the ductile underlying metal.

A group of eight different alloys have been examined at 25°C and 500°C using this apparatus. Results on the erosion loss of the alloys using two different sizes of Al_2O_3 particles are shown in Table 4. The particle velocity was 30 m/s at 45° angle of attack using CO_2 propellent.

Table 4

Erosion Measurements on Alloys Using Two Sizes of Al_2O_3 Particles at 30 m/s and 45° Incidence

Alloy Type	Wt. Loss(mg)/Wt.Abr.(g)				Penetration(μm)/Wt.Abr.(g)			
	25°C		500°C		25°C		500°C	
	5 μm	50 μm	5 μm	50 μm	5 μm	50 μm	5 μm	50 μm
18Ni-250MS	0.08	0.12	0.04	0.95	10	9	0.5	16
AISI 446	0.05	0.05	0.01	0.20	10	6	0.6	11
AISI 304	0.05	0.47	0.02	0.26	7	26	0.2	12
AISI 316	0.04	0.10	0.01	0.21	7	9	0.8	13
AISI 310	0.03	0.09	0.02	0.20	5	9	0.8	13
Incoloy 800	0.06	0.32	0.01	0.26	8	20	0.4	18
Inconel 601	0.06	0.30	<0.01	0.19	8	20	0.4	14
Inconel 671	0.02	0.11	0.01	0.15	4	9	0.4	13

Both relative weight loss and penetration are shown. It is clear that erosion increases significantly with particle size at both temperatures and for all alloys. This size effect is particularly large for the 500°C tests where a decreased erosion loss is seen for all alloys for the 5 μm particles (relative to 25°C). Apparently the developing oxide scale on the surface offers significant protection but only for the small particle size. The data at 500°C using 50 μm size particles varies among the alloys in comparison with the 25°C results. At 500°C the alloys having larger chromium content in general show the least erosion loss (although exceptions are present). Oxide thicknesses measured on specimen cross sections after testing at 500°C for 2 minutes ranged from about 2μm down to less than 0.5 μm, depending on the alloy. More data needs to be acquired at other exposure conditions of velocity, particle size, and environment before definitive conclusions can be reached concerning relative material erosion rates.

A comparison between the results obtained with different abrasives is shown in Table 5. The data refer to 304 stainless steel in air at

Table 5

Erosion Measurements on 304 Stainless Steel Using Different Abrasives at 30 m/s and 45° Incidence

Abrasive (Size)	Wt. Loss (mg)/ Wt. Abr. (g)		Penetration (μm)/ Wt. Abr. (g)	
	25°C	500°C	25°C	500°C
Al_2O_3 (5 μm)	0.5	0.2	7	0.2
Al_2O_3 (50 μm)	0.47	0.26	26	12
Pumice 4F (5-50 μm)	0.21	0.04	29	2.7
Pumice F (5-100 μm)	0.10	0.03	8	1.7
Silica (5-50 μm)	0.50	0.21	45	12

30 m/s particle velocity at two temperatures, 25°C and 500°C. The increased erosion loss for 50 μm Al_2O_3 relative to 5 μm Al_2O_3 particles is apparent. The two grades of pumice show somewhat reduced losses relative to 50 μm Al_2O_3 that are probably associated with the reduced hardness value. However, a detailed study of these and other data shows that factors other than abrasive hardness are significant. These include "cutting efficiency" at elevated temperatures, tendency to fracture, hardness at temperature, etc. Such details can only by understood as a result of comprehensive studies of the various abrasives. Another relevant abrasive characteristic is the tendency for certain abrasives to sinter to the eroded surface and hence offer protection.

Studies of the effect of surface hardness of the metal on erosion resistance are underway. The results of one series of tests are shown in Fig. 5 using SiO_2 abrasive and type 18Ni-250MS steel hardened to different levels. Relatively little effect on erosion rate is seen as the metal hardness varies; that observation has been reported previously by others [14].

Studies at 1000°C: Experiments conducted in the second erosion system have used either 150 μm size SiC abrasive or 50 μm Al_2O_3 particles. Two different types of experiments were conducted. In one, multiple alloy specimen packages were used in order to obtain data on relative erosion for the alloys. In the other, a single alloy specimen was used for each test. Figure 6 shows an example of a multiple alloy specimen package after exposure in the test unit at 1000°C for 60 minutes using

150 μm SiC particles at a velocity of 50 m/s. Excess oxygen conditions were maintained during the test. Each specimen in the package was 0.5 mm thick and was fabricated to have two surfaces exposed to the particle stream at angles of 90° and 45°. Fiducial marks were placed on each specimen surface in order to measure the dimensional loss after testing One other edge, not exposed to the abrasive particles but exposed to the heated atmosphere, provided information on the oxidation process. While this specimen design provides an opportunity for obtaining relative data between the alloy samples in the same atmosphere, there can be interferences between neighboring specimens in the package, particularly if the erosion rates differ greatly. In Fig. 6 the specimens in Inconel 601, 671 and 310 stainless steel exhibit the least erosion. On cooling to room temperature the oxide scale spalled from the 304 stainless steel specimen. Little or no spalling occurred on the other alloys.

Erosion data obtained from two tests using the multiple specimen package under different environmental conditions are shown in Table 6.

Table 6

Erosion Measurements on Alloys at 1020°C in Combustion Gases at Approximately 55 m/s Using 150 μm SiC Particles

	Equivalent Wt. Loss (mg)/Wt. Abrasive (g)			
	Excess Oxygen[1]		Excess Propane[2]	
Alloy Type	90°	45°	90°	45°
AISI 446	0.41	0.35	0.73	1.1
AISI 304	0.59	0.37	1.6	1.5
AISI 316	----	----	1.2	1.3
AISI 310	0.32	0.28	0.58	0.64
Incoloy 800	0.42	0.32	0.56	0.64
Inconel 601	0.29	0.24	0.23	0.49
Inconel 671	0.26	0.28	0.15	0.25

1. Typical Analysis: O_2=13%, CO_2=10%, N_2=64%, H_2O=13%
2. Typical Analysis: H_2=8%, CO=12%, H_2O=17%, CO_2=5% N_2=52%, Other=6%.

Examination of the results in the excess oxygen atmosphere indicate a small difference between the 45° and 90° surface erosion losses. However, under excess propane combustion conditions a greater difference develops between the erosion rates at these two angles. The increased loss at 45° associated with the ductile behavior is clear under excess propane conditions. The difference in erosion rate among the different metals is also more apparent under those conditions. The most resistant

alloys appear to be those containing larger chromium concentrations. That same characteristic appears to apply in more strongly oxidizing atmospheres. An example of the surface conditions that develop at 1000°C after erosion is shown in Fig. 7a for 310 stainless steel exposed under excess oxygen conditions. Much roughening due to impact damage is evident on the surface and some abrasive particles (or fragments) are seen imbedded in the specimen. A cross section through this specimen is shown in Fig. 7b and indicates the oxide film present.

Summary

1. Two sets of test apparatus have been developed and applied to erosion measurements on metals in the temperature range of 25°C to 1000°C. The atmosphere, particle size and velocity, specimen orientation and other significant variables can be controlled.
2. Significant effects on the erosion rates of the metals studied are attributed to the oxide film or scale that forms on the surface. The chromium content of the alloy is one important parameter.
3. Abrasive hardness is a significant factor in erosion rate although other abrasive characteristics may be equally important. Hardness for a given alloy may not be an important parameter.
4. The maximum rate of erosion occurs at angles of 10° to 20° at temperatures up to 500°C, suggesting that cutting processes are a prominent metal removal mechanism.

Acknowledgements

This study was partially supported by the Energy Research and Development Administration/Fossil Energy and their support is gratefully acknowledged. Many useful discussions concerning these studies were held with S. Wiederhorn, D. E. Roberts, E. Passaglia, and others at NBS to whom the authors are indebted.

REFERENCES

1. Neilson, J. H. and Gilchrist, A., "Erosion by a Stream of Solid Particles," Wear, Vol. 11, 1968, pp. 111-122.
2. Goodwin, J. E., Sage, W., and Tilly, G. P., "Study of Erosion by Solid Particles," Proc. Inst. Mech. Engrs. (London), Vol. 184, 1969, pp. 279-292.
3. Kleis, I. R., "Problems der Bestimmung des Straheverscheisses bei Metallen," Wear, Vol., 13, 199 (1969).
4. Sheldon, G. L., "Similarities and Differences in the Erosion Behavior of Materials," Trans. ASME, Vol. 92, 1970, pp. 619-626.
5. Finnie, I., "Some Observations on the Erosion of Ductile Metals," Wear, Vol. 19, 1972, p. 81-90.
6. Tilly, G. P., "A Two Stage Mechanism of Ductile Erosion," Wear, Vol. 23, 1973, pp. 87-96.
7. Tilly, G. P., "Erosion Caused by Airborne Particles," Wear, Vol. 14, 1969, pp. 63-79.
8. Smeltzer, C. E., Gulden, M. E., and Compton, W. A., "Mechanism of Metal Removal by Impacting Dust Particles," Trans. ASME, Vol. 92, 1970, pp. 639-654.
9. "Workshop on Materials Problems and Research Opportunities in Coal Conversion: Conclusions and Recommendations," Staehle, R. W., Director, Ohio State University, April 16, 1974.
10. Hutchings, I. M. and Winter, R. E., "Particle Erosion of Ductile Metals: A Mechanism of Material Removal," Wear, Vol. 27, 1974, pp. 121-128.
11. Roberts, A. G., "Improved NBS Abrasive Jet Method for Measuring Abrasion Resistance of Coatings," ASTM Bulletin No. 244, 1960, pp. 48-51.
12. Wiederhorn, S. M. and Roberts, D. E., "A Technique to Investigate High Temperature Erosion of Refractories," Bull. Am. Ceram, Soc., Vol. 55, 1976, pp. 185-189.
13. Ruff, A. W. and Ives L. K., "Measurement of Solid Particle Velocity in Erosive Wear," Wear, Vol. 35, 1975, pp. 195-199.
14. Finnie, I., Wolak, J., and Kabil, Y., "Erosion of Metals by Solid Particles," Journal of Materials, Vol. 2, No. 3. 1967, pp. 682-700.

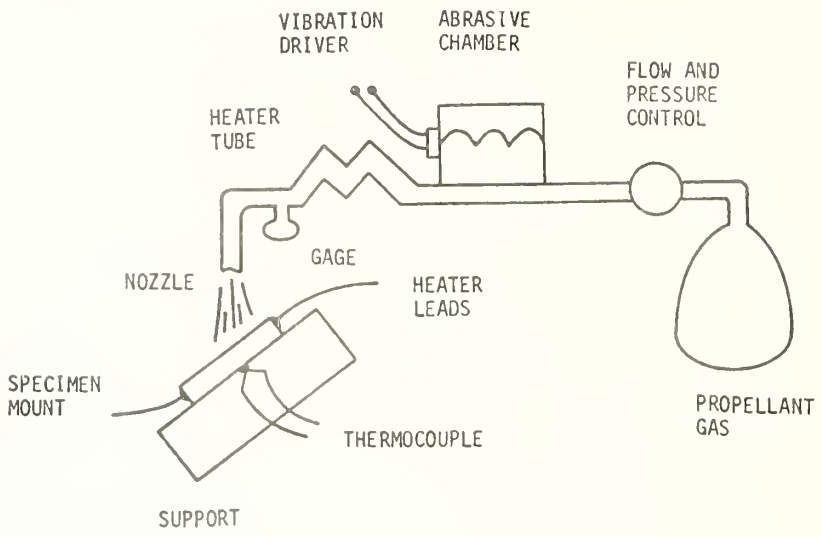

Fig. 1 Schematic representation of the modified Roberts erosion appartus.

Fig. 2 Examples of 5 μm sized Al_2O_3 abrasive particles.

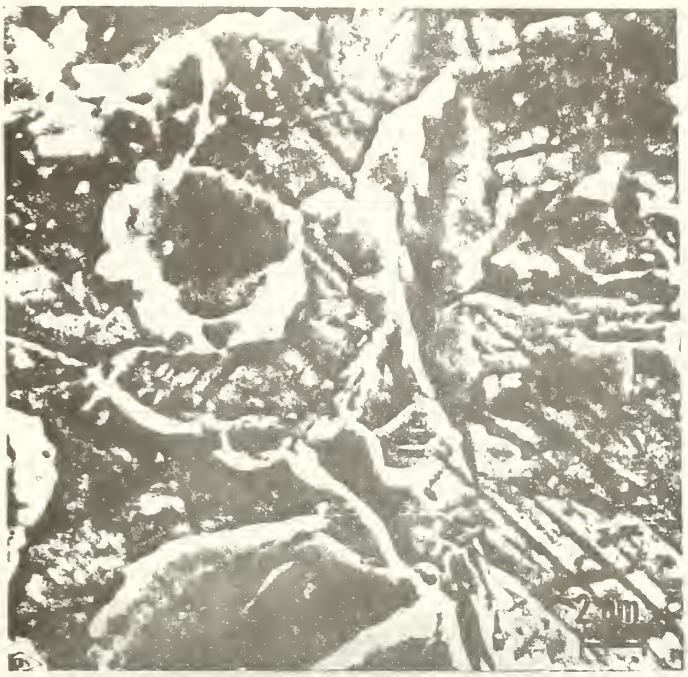

Fig. 3 Erosion impact craters on steel surface.

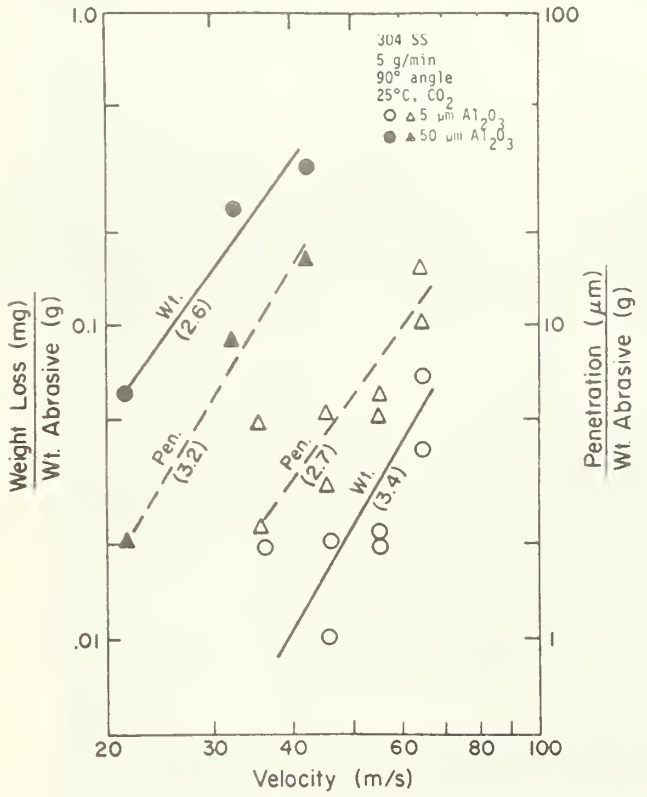

Fig. 4 Velocity dependence of erosion loss at 25°C for two particle sizes.

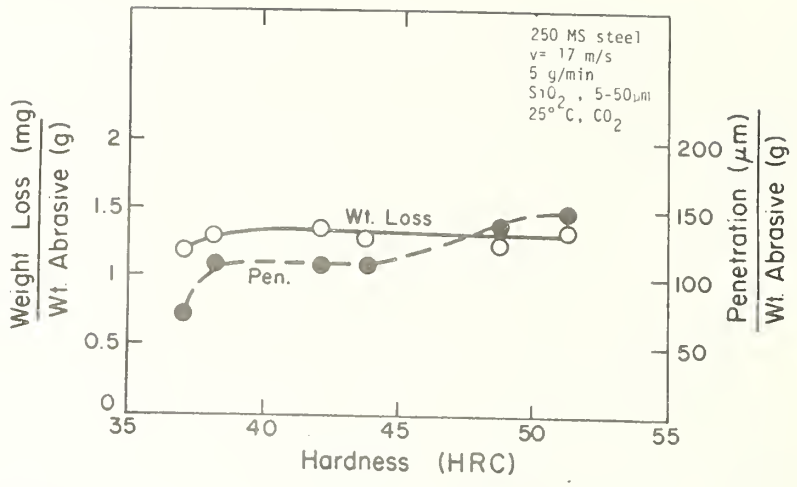

Fig. 5 Variation of erosion loss for different hardness levels in type 18Ni-250MS steel.

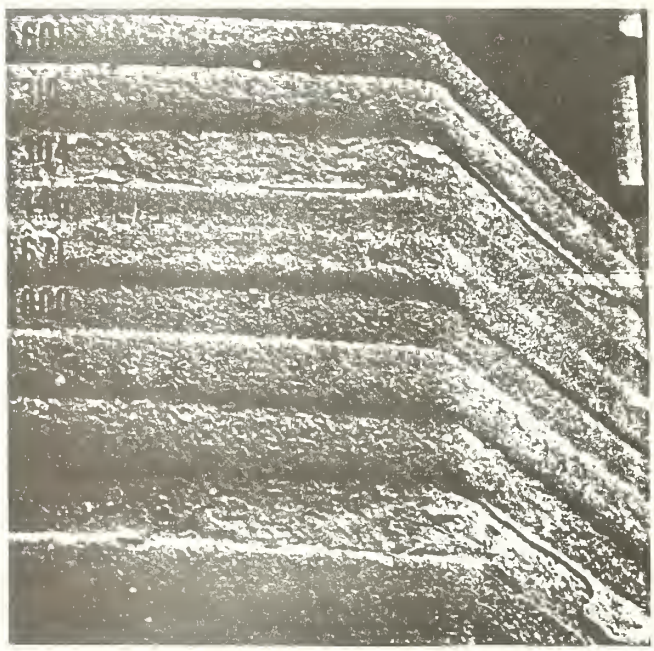

Fig. 6 Multiple alloy specimen package after erosion test at 1000°C. Two exposed surfaces 45° and 90°, are shown.

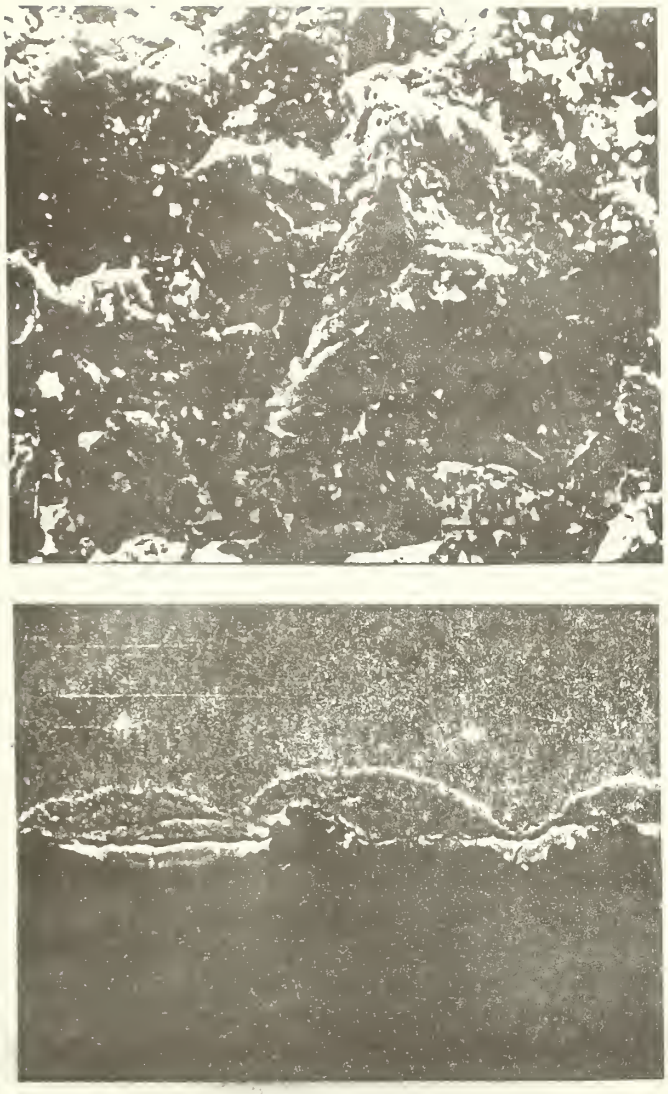

Fig. 7
(a) Surface of 310 stainless steel after erosion test at 1010°C.
(b) Cross section of specimen showing oxide film and erosion craters.

B. Ceramics

(a) Deformation and Fracture (E. R. Fuller, Jr., C. R. Robbins and J. M. Bukowski, 313.05)

Progress: High-pressure steam, one of the reactants used in the gasification of coal, has been found to interact with the bonding phases of several castable refractories used as liners in coal gasifiers. In some instances, these interactions disrupted the bonding structure, thus, adversely affecting the structural integrity of the castable. To examine these effects, measurements of the flexural strength of these materials have been performed at room temperature subsequent to hydrothermal exposure. Mineral phase transformations resulting from the hydrothermal treatment was monitored by x-ray diffraction analysis. High-pressure steam was found to have a dramatic effect on a high-purity, calcium-aluminate-bonded castable and on high-purity, calcium aluminate cements. The flexural strength of these materials decreased sharply after hydrothermal exposures at temperatures above approximately 350°C. This degradation of mechanical properties appeared to be related to the formation of a high-pressure, calcium-aluminate hydration phase, $C_4A_3H_3$ in the cement matrix that bonds the alumina aggregate, and to the dehydration of other bonding phases.* In contrast to this behavior, a calcined flint clay castable was found to be mechanically unaffected by hydrothermal treatment. Additional bonding phases in the cement matrix appeared to maintain the integrity of this castable for the hydrothermal conditions which were examined.

The room temperature bend strength subsequent to hydrothermal treatment for these two commercial refractories is plotted in figures 1 and 2 versus the hydrothermal treatment temperature. The nature of this effect has been examined further in the past quarter. Polished sections of these commercial castables were examined subsequent to hydrothermal exposure using both optical and scanning electron microscopes. Chemical compositions of various mineral phases were determined with energy dispersive x-ray analysis. These results were correlated with the mineral phases that have been identified by x-ray diffraction analysis. See Table 1. These transformations are the result of chemical reactions between the high-pressure steam and the ceramic components of the castable refractories. After firing and prior to hydrothermal treatment, the high-purity, calcium-aluminate castable refractory contained only alumina and calcium-aluminate phases. Hydrothermal treatment results in the formation of several hydrated alumina and calcium-aluminate phases. As the hydrothermal treatment temperature increases these phases undergo several dehydration steps (as listed in Table 1). Until the formation of the $C_4A_3H_3$ phase, these hydration phases are ones commonly observed during mixing and curing of these castables. The strength degradation appears to be associated with the formation of this high-pressure hydration phase of calcium aluminate and

---

* Cement chemistry notation used throughout this section is:

A = Al_2O_3; C = CaO; S = SiO_2; and H = H_2O

to the dehydration of boehmite (AH), which was formed in the refractory at lower temperatures. With the dehydration of C_3AH_6 and the formation of $C_4A_3H_3$, the boehmite apparently acts as a predominant bonding phase in the matrix of the refractory, providing substantial strength to the matrix. However, when this phase decomposes, the bonding matrix loses its structural integrity which appears to cause the decrease in the after-exposure strength. Examination of polished sections with a scanning electron microscope revealed the crystallization of the $C_4A_3H_3$ phase in the bonding matrix, thus disrupting the bonding.

In contrast to this behavior, the calcium-aluminate cement with calcined flint clay aggregate did not react with steam to form predominantly this hydrated calcium-aluminate phase. Instead high-pressure steam appears to accelerate the reaction between the calcium-aluminate phases which are initially present, and the fine calcined flint clay aggregate to form a calcium alumino-silicate, anorthite (CAS_2), that maintains the strength of the bonding matrix. The anorthite, a feldspar mineral commonly found in igneous rocks, forms a strong continuous structure that penetrates throughout the refractory matrix and into some of the larger aggregates firmly holding these coarse aggregates in place. The high strength of this calcined flint clay refractory is attributed to this structure of the matrix.

These environmental effects on the bonding matrix have been further verified by examination of sized fractions of these commercial refractories (+150 mesh and -150 mesh). The -150 mesh fraction of each refractory were cast into specimens and their flexural strength determined after exposure to hydrothermal environments. See Figure 3. Again we see that the high-purity, calcium-aluminate refractory exhibits a strength degradation; whereas the calcined flint clay castable maintains its integrity, confirming the previously determined results. In addition to examining the cement matrix, effect of hydrothermal environment on the alumina aggregate have been investigated. The room temperature bend strength of three densities of sintered alumina were examined subsequent to hydrothermal treatment. See Figure 4. With increasing hydrothermal treatment temperature each type of sintered alumina exhibited a strength loss that appears to be related to the density, or porosity. However, no mineral phase changes were detected from the x-ray diffraction analysis. It is speculated that steam attacks the grain boundaries to form grain-boundary hydration phases, thus weakening these sintered alumina specimens.

These studies demonstrate the importance of chemical reactions and phase transitions in castable refractories intended for use as liners in coal gasification plants. Reactions that form weak phases seriously degrade the mechanical properties of the liner, and significantly decrease its expected lifetime in service. Thus far, the importance of water as a reactive species has been demonstrated. However, since other gases in coal gasification environments are likely to cause similar degradation of strength, it is important to identify chemical reactions that can

occur between these gases and the refractories. Toward this objective three pressure vessel systems are presently being developed: two for exposure testing with subsequent mechanical property characterization; and one for mechanical properties testing under coal gasification conditions. The specifications and properties of these pressure vessels are listed in Table 2. System 2 for exposure testing is a commercial system which has been ordered. The projected delivery date is the latter part of July 1976. The other system for exposure testing (system 1) is a modified in-house pressure vessel. It is presently operational and is being used with CO_2 and/or steam in experiments described below. However, further minor modifications are necessary for the introduction of other gaseous environments and for the venting of obnoxious gases. A gas manifold and venting system are being developed for this purpose. A major consideration in the construction of the manifold and venting system is the ease of adaptability to the other two pressure vessel systems. Preliminary design of pressure vessel system 3 for *in situ* mechanical properties testing has been completed. Basically this system is a two pressure vessel system. The inner pressure vessel is a hot-walled pressure vessel containing the coal gasification environments. This vessel is contained in a room temperature pressure vessel which will be pressurized to the same pressure so as to support the inner vessel. Long-lead-time items for the construction of the outer vessel have been ordered.

To provide some quality control over the refractories which are tested, three laboratory refractory compositions are being prepared for these studies. These compositions - two calcium-aluminate-bonded and one phosphate-bonded - are typical of the spectrum of refractories expected for use as liners in coal gasification systems. The two calcium-aluminate-bonded refractory compositions will be similar to the two commercial refractories previously studied. One will contain tabular alumina aggregate with a high-purity calcium aluminate cement; and the other will contain calcined kaolin aggregate with the same calcium aluminate cement. The third refractory composition, a phosphate-bonded refractory, will contain a tabular alumina aggregate and will be bonded by phosphoric acid. The components to form these refractory compositions have been obtained and the refractory aggregates graded into various size fractions. The calcined kaolin refractory composition has been prepared from calcined kaolin aggregate and calcium-aluminate cement in the following weight percents: coarse aggregate - 65% calcined kaolin (+ 325 mesh) graded into various size fractions; fine aggregate - 10% calcined kaolin (- 325 mesh); and 25% of a calcium-aluminate cement. The resulting refractory has a chemical composition of approximately 56% alumina, 37% silica, 4.5% lime and 0.8% iron oxide. Refractory specimens, prepared from this mixture and fired according to standard practices, have a control flexural strength of approximately 1,300 $\pm$ 350 psi. Investigation of the mechanical properties after exposure to CO_2 and CO_2/steam environments has begun for this composition. Experiments performed thus far were run at 610°C and 1000 psig total pressure. With a pure CO_2 atmosphere, 65 hour exposure resulted in little change in strength; the after-exposure bend strength was 1,200 $\pm$ 220 psi. However, when the environment consisted of 50% CO_2 and 50% steam the strength approximately doubled. This has been verified in both a 20 hour exposure test and a 165 hour exposure test which had after-exposure

bend strengths of 2,170 ± 380 psi and 2,180 ± 440 psi, respectively. X-ray analysis of the chemical phase is still in progress at this time. Preliminary results suggest that this increase in strength is related to an enhanced crystallization of anorthite (CAS_2) and $CaCO_3$ ($C\overline{C}$).

Plans: Mechanical properties testing after exposure to environments of CO_2 and CO_2/ steam at elevated temperature and pressure will be continued. Design and construction of pressure vessel barricades, gas manifold, and venting system for obnoxious gases will also be continued. These systems will be applicable to all three of the pressure vessel systems. The design of the internal pressure vessel and the loading system for the *in situ* system (system 3) will be completed, components ordered, and construction begun on this part of the system.

Table 1. Predominant Phases, as Determined by X-Ray Diffraction Analysis, Subsequent to Hydrothermal Treatment. Phases Listed in Apparent Order of Abundance.

Temperature	High-purity alumina castable	Calcined flint clay castable
Room Temperature	α-Alumina (α-A) CA, CA_2	Mullite (A_3S_2), Cristobalite, α-Alumina (α-A), CA_2, Anorthite (CAS_2), CA, Amorphous Phase
110°C (230°F)	α-A, C_3AH_6, Gibbsite (AH_3)	Cristobalite, A_3S_2, α-A, Gibbsite (AH_3), C_3AH_6, CAS_2,
210°C (410°F)	α-A, Boehmite (AH), C_3AH_6, $C_4A_3H_3$ (trace)	Cristobalite, A_3S_2, Boehmi (AH), α-A, C_3AH_6, CAS_2, $C_4A_3H_3$
310°C (590°F)		A_3S_2, Cristobalite, α-A, AH, $C_4A_3H_3$, CAS_2, C_3AH_6
350°C (662°F) 375°C (707°F)	α-A, $C_4A_3H_3$	
410°C (770°F) 510°C (950°F)	α-A, $C_4A_3H_3$	A_3S_2, Cristobalite, CAS_2, α-A, Tridymite

Table 2. Specifications and Properties of Pressure Vessels

	For Exposure Test		For *in situ* Test
	System 1	System 2	System 3
max. temperature	600°C	960°C	1010°C
pressure limit at temperature	5,100 psi	3,000 psi	1,000 psi
gauges (max. working pressure)	0-600 psi (450 psi)	0-1500 psi (1125 psi)	0-1500 psi (1000 psi)
	0-2000 psi (1500 psi)	0-3000 psi (2250 psi)	
Dimensions:			
volume	1,000 ml	260 ml	
internal diameter	2.5"	1.3"	4"
internal length	13.13"	11.85"	
length of hot zone	~ 6"	~ 4"	~ 6"
# of vessels	1	2	1
source of steam pressure	closed system; generated from H_2O	water pump	pressurize water system
projected installation	May 76	Aug. 76	Jan. 77
projected operation	June 76	Sept. 76	April 77

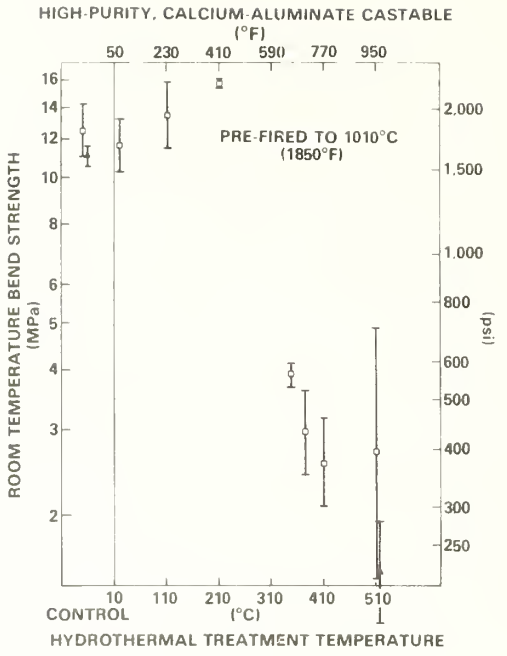

Figure 1. Room Temperature Bend Strength versus Hydrothermal Treatment Temperature for a High-Purity, Calcium-Aluminate Castable

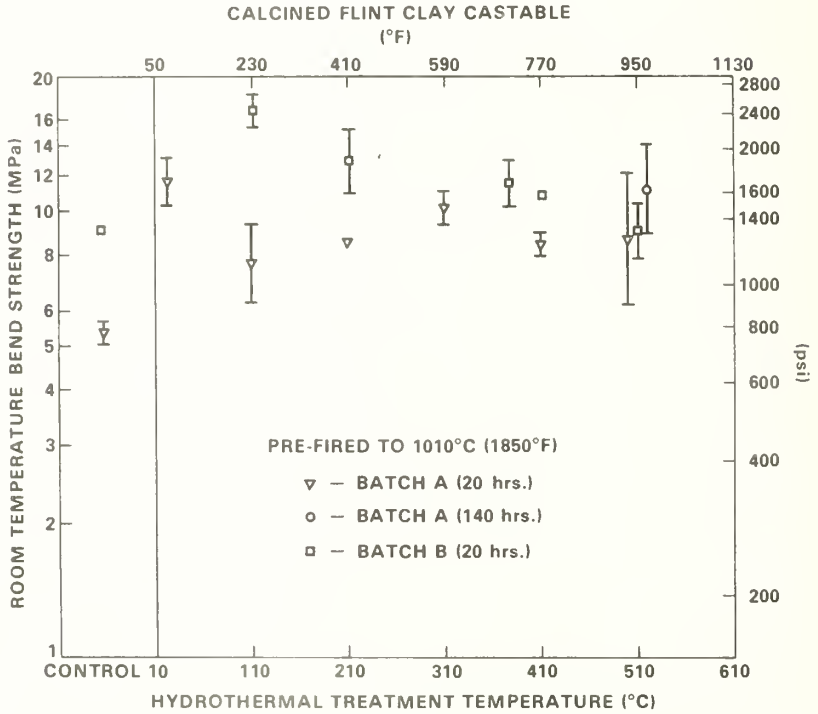

Figure 2. Room Temperature Bend Strength versus Hydrothermal Treatment Temperature for a Calcined Flint Clay Castable.

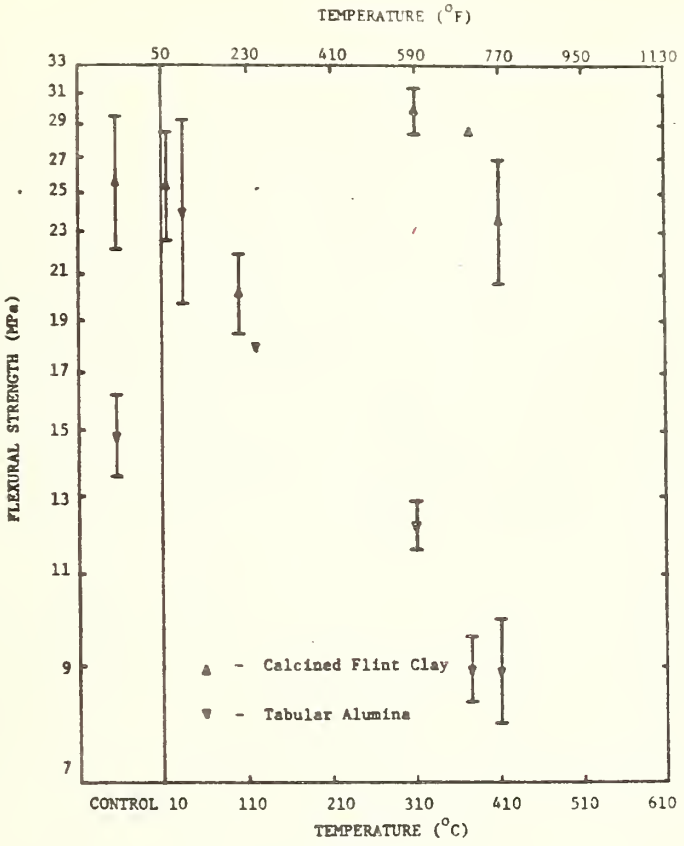

Figure 3. Room Temperature Bend Strength versus Hydrothermal Treatment Temperature for -150 Mesh Fractions of a High-Purity, Alumina Castable and of a Calcined-Flint Clay Castable.

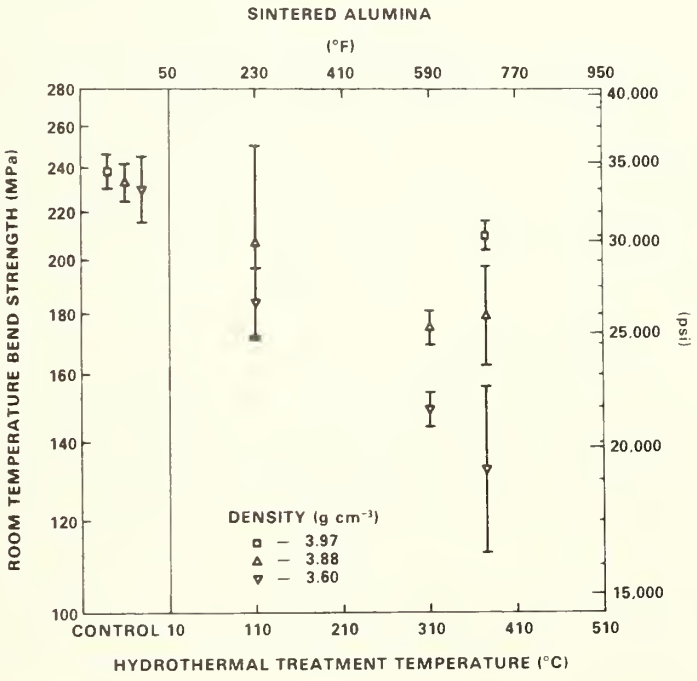

Figure 4. Room Temperature Bend Strength versus Hydrothermal Treatment Temperature for Three Densities of Sintered Alumina.

b. Erosive Wear (S. M. Wiederhorn and D. E. Roberts, 313.05)

Progress: Castable refractories will be used in coal gasification applications where resistance to both chemical attack and erosion is required. Applications will include the linings of major components of gasifier plants such as reaction vessels, hot transfer lines, and cyclone separators. To assure adequate performance in these applications and to accumulate information that can be used by engineers for design purposes, this program is being conducted to characterize the erosion resistance of castable refractories. An important goal of this project is to determine the type of castable refractories that will be both erosion resistant and sufficiently inexpensive to satisfy the economic requirements of coal gasifiers.

With these objectives in mind, this project was initiated to characterize the erosion behavior of castable refractories. In the initial stages of the program an apparatus was developed which could be used to study the high temperature erosion behavior of refractories, in environments that simulate coal gasification environments. The apparatus is capable of temperatures that range from 25°C to 1000°C and of accelerating particles to velocities of from 10 to 100 m/s. This range of temperatures and particle velocities cover the range expected in gasification plants. Although the apparatus was designed to operate at one atmosphere pressure, the environmental composition can be regulated by controlling the input gas composition. An analysis of the gases at the specimen site indicated that the gas composition was similar to that of the Bureau of Mines' gasifier at Morgantown, Pa.

Early studies using this apparatus indicated a rather strong dependence of erosion rate on particle velocity. The erosion rate could be expressed as a power function of the particle velocity, with a power exponent of approximately 3. This value is similar to that reported for other materials. Erosion occurred primarily by wear of the cement phase of the castable refractories in such a manner that channels were often observed to form in the surface of the refractory. As the cement phase was worn away, aggregate grains would fall from the refractory surface resulting in general wear. By increasing the strength of the cement phase (by reducing the water to cement ratio for example) channel formation, and thus wear could be suppressed; conversely, wear could be accelerated by adverse chemical reactions (for example high pressure steam which has been shown to weaken some refractories).

The erosion resistance of a high purity alumina castable refractory was found to increase slightly as the temperature was increased from 25°C to 1000°C. This increase in erosion resistance was accompanied by a change in the erosion mechanism. At 25°C erosion occurred by a brittle fracture process during which small particles of the refractory were chipped from the refractory surface by the abrasive particles. At 1000°C the erosion was controlled by plastic deformation. Evidence for plastic deformation was obtained from optical microscopy and scanning electron microscopy studies, and from investigations of the erosion rate as a function of particle impingement angle. At high temperatures great numbers of erosion particles were observed to become imbedded in the surface of the refractory indicating that the temperatures have softened the refractory to permit a degree of plastic flow.

Further evidence for high temperature plastic flow was obtained from studies of erosion as a function of particle impingement angle. At 25°C the dependence of erosion rate on angle of impingement, Figure 1a, is typical of that found for brittle ceramic materials such as porcelain: the erosion rate is maximal at 90° impingement and decreases slowly as the angle of impingement decreases. At 1000°C, the erosion behavior, Figure 1b, is similar to that reported for metals: the erosion rate is minimal at 90° and increases as the angle of impingement decreases passing through a maximum at approximately 20° before decreasing to zero. As will be seen in the discussion given below, this high temperature behavior is modified by the development of surface channels.

During the past year the results discussed above were extended by investigating the effects of hydrothermal environments on the erosion of castable refractories. Two types of refractories were used in the investigation. One was a high purity aluminum oxide refractory consisting of tabular alumina bonded with a calcium aluminate cement. The other was a calcined flint clay aggregate also bonded with calcium aluminate cement. Cubes of these refractories, 1/2 inch on a side, were hydrothermally treated by sealing them in a fixed volume (20 cc) Morrey bomb that contained approximately 3 cc's of water. The bomb was placed in a furnace which had been pre-heated to the temperature of reaction. After 20 hours of exposure the bomb was removed and permitted to cool to room temperature. Specimens were then removed from the bomb and dried in air. The erosion studies were conducted at room temperature to determine if the erosion properties of these materials had been changed by the hydrothermal treatment. Each specimen was eroded by 100 grams of 100 mesh silicon carbide particles, at velocities that ranged from 15 to 50 m/s. The erosion rate was determined from weight loss measurements after exposure.

This study demonstrated a susceptibility of the high alumina castable refractory to chemical attack under the conditions of test. Below 200°C exposure, the erosion resistance of the high alumina castable was essentially unaffected by the hydrothermal treatment (Figure 2a). At approximately 300°C the erosion rate of this castable refractory increased by a factor of 10, indicating a significant change in its erosion resistance. By contrast the erosion resistance of the calcined flint clay castable was unaffected by the hydrothermal treatment over the temperature range 25°C to 500°C (Figure 2b). A comparison was made between the erosion resistance and the strength of castable refractories that received similar hydrothermal treatments. Over the same temperature range, the strength of the high alumina castable refractory decreased precipitously at 300°C. Whereas the strength of the calcined flint clay castable refractory was unaffected by hydrothermal treatments.

In order to determine the cause of the change in strength and erosion resistance, an X-ray analysis was done of the castable refractories after the hydrothermal treatments. The strength degradation and enhancement of the erosion rate appear to be associated with the formation of a high pressure hydration phase of calcium aluminate ($4CaO.3Al_2O_3.3H_2O$) and the dehydration of boehmite which forms in the

refractory temperatures between 110°C and 210°C. With the dehydration of $3CaO.Al_2O_3.6H_2O$ above 210°C and the formation of $4CaO.3Al_2O_3.3H_2O$, the boehmite apparently acts as the predominant bonding phase in the matrix and provides substantial strength to the refractory. However when this phase decomposes, the bonding matrix loses its structural integrity resulting in the observed decrease in both the strength and erosion resistance of the refractory.

In contrast the above behavior, the calcined flint clay refractory did not react with steam to form a low strength hydrated calcium aluminate phase. Instead the calcium aluminate that was initially present reacted with the mullite aggregate to form calcium alumino-silicate phases that maintained their strength. One of the calcium alumino-silicate phases was anorthite, a feldspar type of mineral commonly found in igneous rocks. Although highly porous, the calcium alumino-silicate phases formed a strong structure that penetrated throughout the refractory firmly holding the mullite aggregate in place. It is this matrix that accounted for the high strength and erosion resistance of the calcined flint clay refractory.

This study demonstrated the importance of chemical reactions and phase transitions to mechanical properties. Reactions that form weak phases will seriously degrade the mechanical properties of linings and significantly decrease their expected lifetime in service. In this study the importance of water as a reactive species was demonstrated. However since other gases in coal gasification environments are also likely to cause degradation of strength and erosion resistance, it is important to identify the chemical reactions that occur between these gases and the refractories. Therefore one objective of future work will be to identify other chemical reactions that are detrimental to the mechanical integrity of the refractories.

In more recent work, the effect of long term exposure on erosion rate was also investigated. This study was conducted to determine the effect of surface topology on the erosion rate. As erosion occurs in refractories, the cement matrix that holds the aggregate particles together is slowly worn away. The result of removing matrix material is to leave open channels within the castable refractories. In earlier phases of this project small amounts of abrasive were used and as a result wear in the matrix material was often not fully developed. Therefore it was felt essential to determine erosion rates on castable refractories under conditions in which fully developed channels formed in the castable refractory so as to evaluate the erosion properties of these refractories after long term use.

The study of long term wear was conducted by exposing castable refractories to an erosive stream at relatively high velocities, 70 to 90 m/s. The high velocities were used so that channeling would develop in a relatively short

time. The study was conducted both at 25°C and at 1000°C. In order to determine if the erosion rate changed as the surface topology evolved, the experiment was conducted using increments of 25 grams of abrasive for the first 100 grams of exposure, 50 gram increments for the next 200 grams of exposure and 100 gram increments for the final 300 grams of exposure. Each specimen was exposed to a total of 600 grams of abrasive. In order to determine if the erosion rate depended on the incident angle of particle impingement, the castable refractories were exposed at angles ranging from 15° to 90°. Specimens for these angular studies were pre-cut so as to expose the surface at the correct angle.

In both the high and low temperature studies the erosion rate was found to initially decrease as the amount of abrasive used was increased and then to approach a steady state (Figure 3 and 4). The change in the initial erosion rate was not as great for the studies at 25°C as for those at 1000°C. For impingement angles of less than 45°, there was little change in the erosion rate at 25°C as the amount of abrasive was increased. By contrast at 1000°C the erosion rate for the first 25 gram increment of exposure was considerably greater than that observed in subsequent exposures. This change in the rate of erosion can be attributed to the development of a steady state surface structure. For the room temperature studies the surface remained relatively flat during exposure. By contrast the surfaces at 1000°C had deep channels around the abrasive particles.

The results of the 25°C study differed from an earlier one in which deep channels were observed to form around the aggregate particles. It is felt that this difference arises from the method of making the refractories, which had changed from the earlier method. Refractories are now made using a cement mixer and small amounts of water, whereas the earlier refractories were hand mixed using larger amounts of water. The change in the erosion rate of the material suggests that an increase in the water-to-cement ratio reduces the erosion resistance of the cement, permitting channels to form. This finding is in agreement with earlier findings in the literature. The results of the current study also suggest that if the water-to-cement ratio can be reduced sufficiently, then the cement matrix can be made nearly as erosion resistant as the aggregate particles, resulting in a greater resistance to erosion.

At high temperatures, however, the fact that the cement matrix becomes plastic, reduces its effective erosion resistance, and results in the formation of deep channels. It is interesting that these channels are formed regardless of the direction of impingement. The structure of the channels reflect the angle of impingement. Thus at 90° exposure the channels go straight down into the refractory while at low angles of exposure, the channels lie at an angle to the surface. The presence of erosion resistant aggregate particles have the effect of modifying the appearance of the refractory surface and of protecting the surface from erosion.

The effect of angle of impingement on the erosion rate is shown in Figure 5 for studies at 25°C and 1000°C. The erosion rate changes only slightly with the impingement angle. At room temperature the erosion rate decreases by a factor of approximately 20% as the angle impingement is changed from 90° to 15°. At 1000°C the erosion rate is relatively constant between 90° and 30°, and then drops by a factor of about 2 at 15°. The low temperature behavior (Figure 5a) is similar to those reported earlier (Figure 1a) where only 100 grams of abrasive were used, and where relatively low particle velocities were used (20 m/s). At 1000°C the behavior in Figure 5b differs considerably from that shown in Figure 1b. It is believed that the shape of the curve obtained in this figure reflects the fact that the surface topology was different in the two studies. The development of deep channels in the present study modifies the erosion behavior. While the erosion still occurs by a ductile flow mechanism, the formation of channels and steps on the surface effectively results in a 90° exposure angle for all angles used. This is illustrated in Figure 6 where the erosion was shown schematically in two dimensions. During the very initial stages of erosion the surface is flat but as the cement matrix erodes away pockets are formed between the aggregate grains. Each of these pockets is aligned normal to the direction of the incoming particles. Therefore the total effect of channel formation in the refractory is to form a surface that lies at 90° to the impingement particles. As a consequence this behavior the erosion rate now becomes insensitive to the angle of impingement. This behavior can have significant practical importance if it holds for other castable refractories, since erosion measurements will not have to be made over a range of impingement angles to characterize the wear of the refractory. Instead a convenient angle can be selected to measure the erosion rate and to completely characterize the erosion resistance as a function of impingement angle. This result further implies that in estimating the rate of erosion for castable refractories in service one can assume the rate of erosion to be dependent of impingement angle.

Plans: During the next year further erosion studies will be conducted to characterize the erosion rate of castable refractories. Target materials will include a phosphate bonded tabular alumina refractory and a calcined Kaolin refractory.

The effect of temperature on the erosion rate will be investigated by exposing refractories to 100 grit silicon carbide particles at temperatures of 25 and 1000°C. Particle velocities will range from 10 to 100 m/s and erosion measurements will be conducted using 90° impact angles. The effect of angle on the erosion rate will also be tested for a selected range of angles. Study will not be as extensive as the one just completed unless some difference in behavior is noted.

Since erosion in gasifiers will be due to particles that are much softer than silicon carbide, studies will also be conducted to evaluate the effect of particle hardness on erosion rate. Dolamite, silica sand, tabular alumina and ground-up coal slag will be used as erosion particles. Studies will be conducted at temperatures of 25° and 1000°C using an impingement angle of 90°. In order to determine the effect of particle size on erosion rate these materials will be sized to form erosion mixes having particle diameters of approximately 50, 150 and 500 micrometers.

In addition to the above studies the hot erosion equipment developed earlier in this project will be suggested as a standard ASTM technique for characterizing the erosive wear of ceramic refractories. The technique will be described at a meeting of ASTM Committee C-8, and if interest is expressed in the technique arrangements will be made to have similar sets of equipment constructed at other laboratories. Round Robin Tests will then be conducted to determine the accuracy of the equipment and its applicability to erosion tests. The adaptation of this technique will provide a uniform standard by which the erosion resistance of castables can be measured.

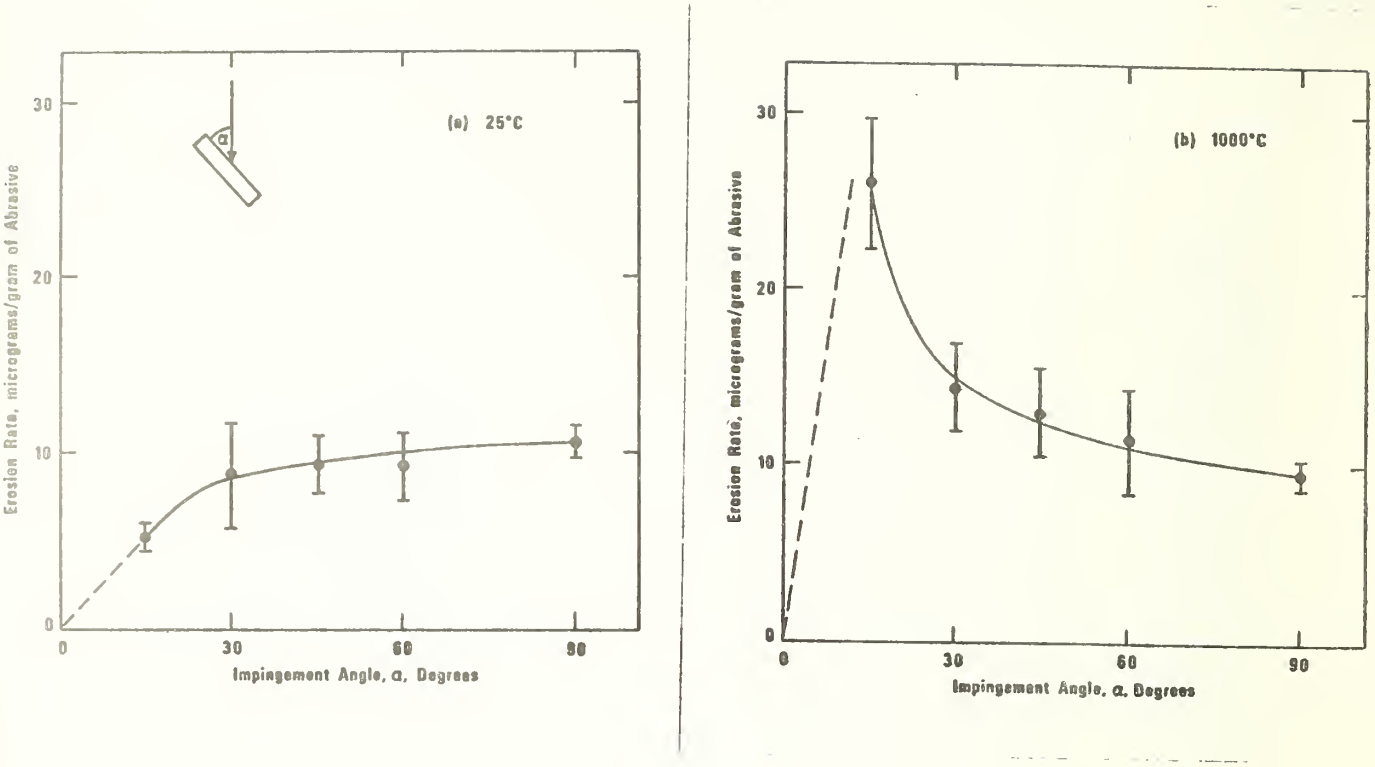

Figure 1. Initial stages of wear. Dependence of erosion rate on the angle of impingement (a) 25°C; and (b) 1000°C. The error bars represent one standard deviation from the mean.

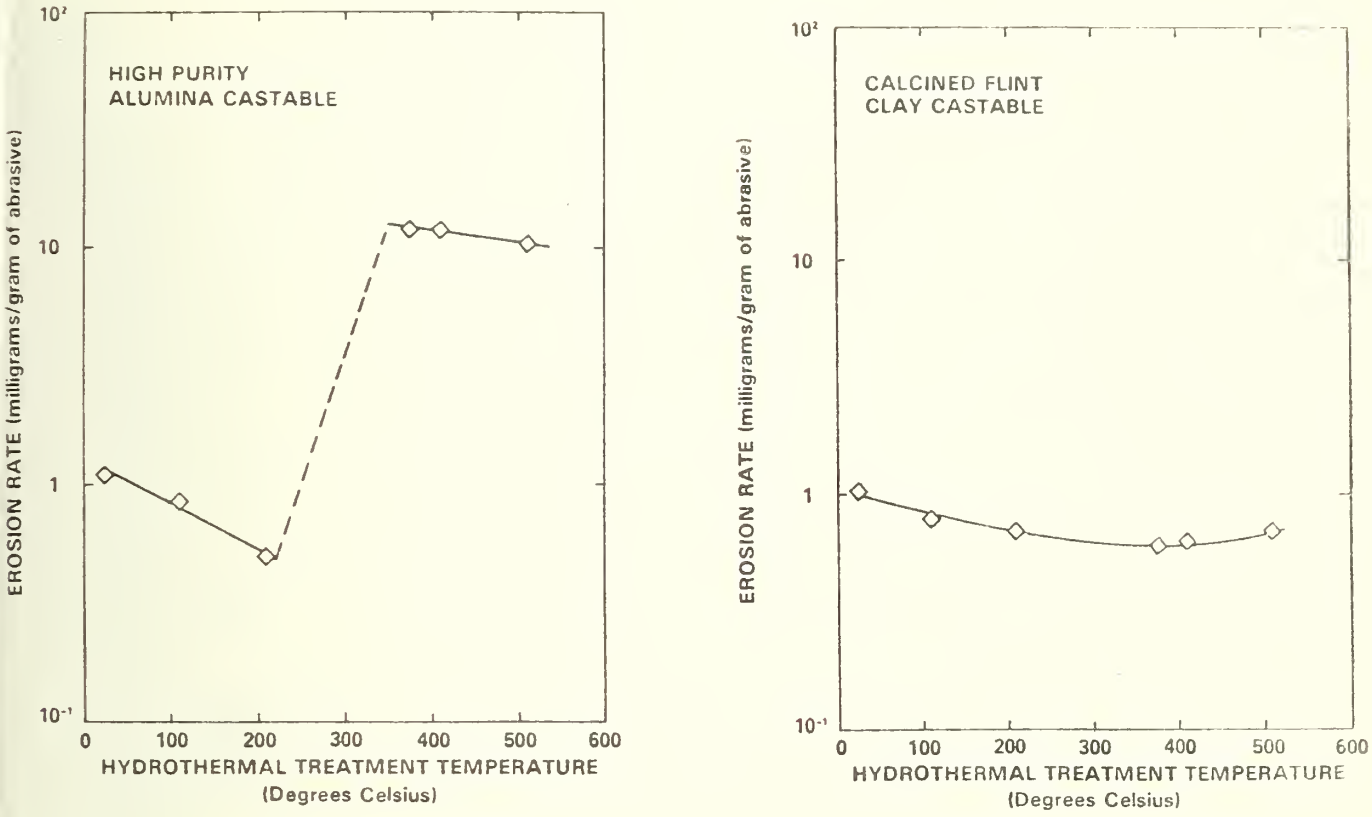

Figure 2. Effect of hydrothermal treatment on the erosive wear of castable refractories. Tests conducted at room temperature after hydrothermal treatment.

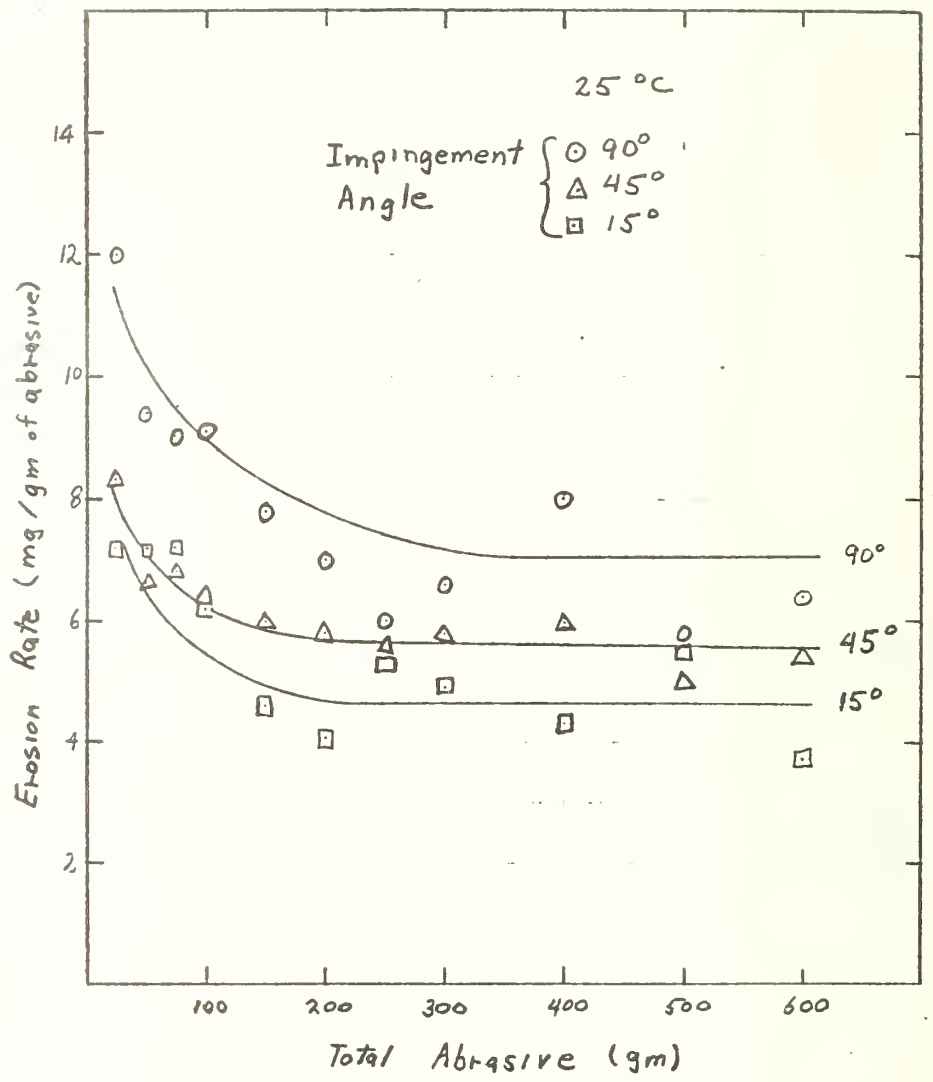

Figure 3. Low temperature erosive wear as a function of the amount of abrasive used.

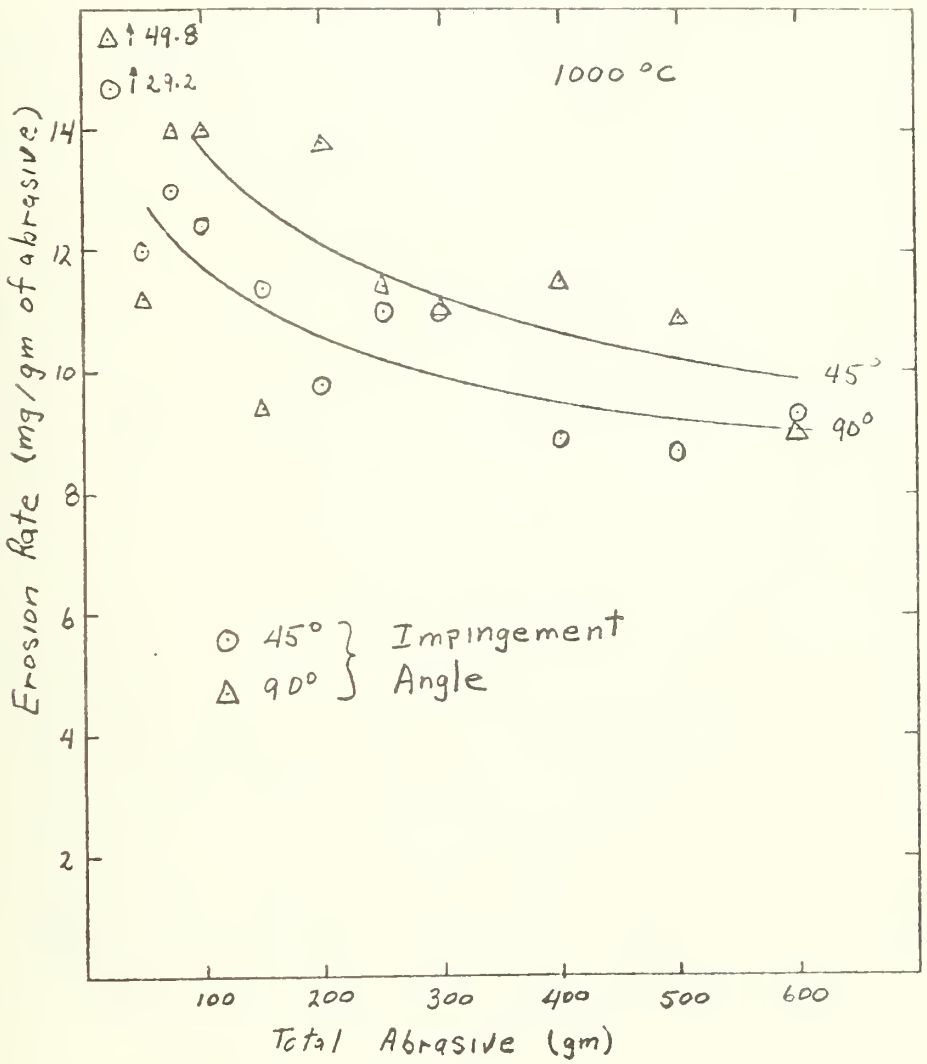

Figure 4. High temperature erosive wear as a function of the amount of abrasive used.

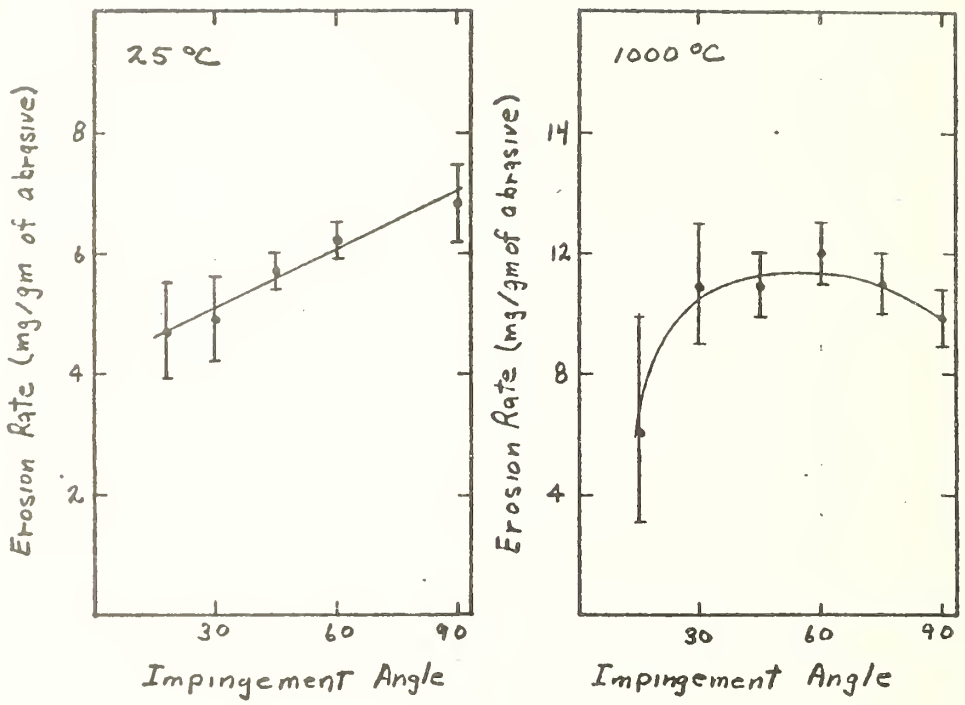

Figure 5. Erosion Rate as a function of impingement angle. Long term erosion with full channel development. High purity aluminum oxide castable refractory bonded with calcium aluminate. The error bars represent one standard deviation from the mean.

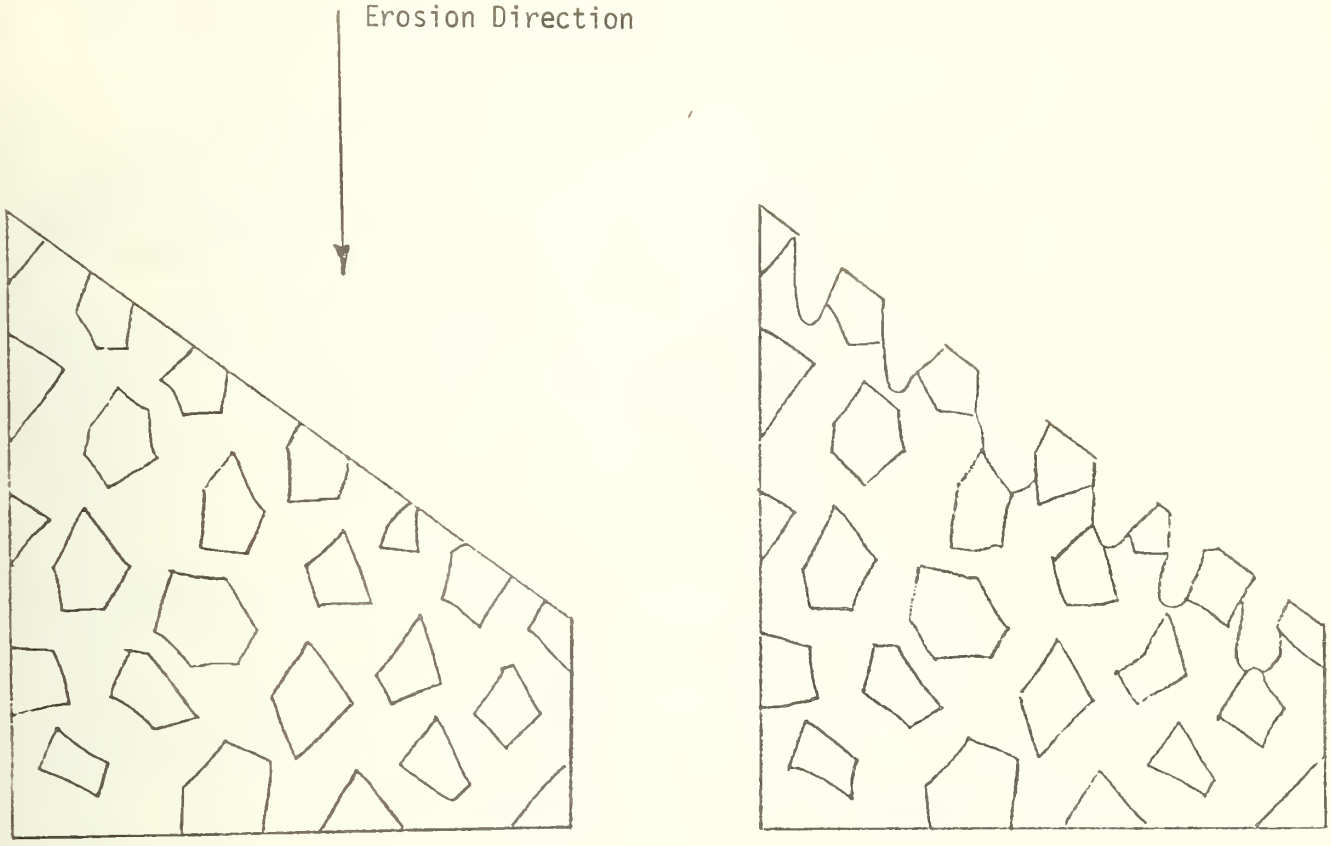

Figure 6. Schematic diagram of channel development. Left-hand figure shows castable refractory prior to erosion. Right-hand figure shows the early stages of wear in which the cement phase is preferentially worn, leaving channels on the surface. Since the bottoms of these channels are aligned perpendicular to the erosion direction, erosion occurs at the same rate as if the original surface were aligned perpendicular to the direction of erosion.

2. Chemical Degradation of Ceramics (W.S. Brower, J.L. Waring and C.A. Harding, 313.03)

a. Gas Phase Reactions

Some work in the $CaO-Al_2O_3-H_2O$ system has been previously reported in the literature. The most outstanding is the work of Peppler and Wells and Majumdar and Roy. For the purposes of studying the solid state reactions encountered with steam in a coal gasifier the solubility work of Peppler and Wells was reinterpreted with the view of integrating the data with that of Majumdar and Roy. This was accomplished by constructing the diagram given in Figure 1 from the data in Table 1. From Figure 1 it can be seen that the various existence regions can be generally characterized. From this preliminary data it was found that the work of Peppler and Wells and Majumdar and Roy can be integrated to predict behavior at 1000°C. Therefore it was necessary only to verify that portion of the system which could directly effect the operation of a coal gasifier at 1000 psi of steam at 1000°C.

A constitution diagram giving the results of this study (Figure 1) has been constructed from the data given in Table 1. From Figure 1 it can be seen that the first hydrate formed $3CaO:Al_2O_3:6H_2O$ is unstable and dissociates above room temperature to form $Ca(OH)_2$ and $4CaO:3Al_2O_3:3H_2O$. Preformed of 1000°C at 1000 psi steam. The 1000°C/1000 psi data was obtained with the TZM apparatus. The maximum and minimum dissociation temperature for the $12CaO:7Al_2O_3$ hydrogarnet have not been established. However the minimum temperature of formation is probably in excess of 400°C and the compound should be stable to the reported melting point of about 1392°C. The hydrate $4CaO:3Al_2O_3:3H_2O$ has a minimum temperature of stability below 200°C and a maximum temperature of stability below 600°C in 1000 psi steam. The $CaO:Al_2O_3$ and $CaO:2Al_2O_3$ were found to exist at temperatures in excess of 1000°C and to hydrate below about 400°C. The compounds $CaO:Al_2O_3$, $CaO:2Al_2O_3$ and $CaO:6Al_2O_3$ experimentally appear to have the same minimum temperature of stability since at these relatively low temperatures the reactions proceed very slowly and it has not been possible to delineate these boundaries, therefore the region of uncertainty is shaded on the diagram. At a temperature below about 400°C-450°C these phases dissociate into boehmite and $4CaO:3Al_2O_3:3H_2O$. The phase transition between boehmite and Al_2O_3 in the pressure range of 1000 psi is currently under investigation.

In conclusion at 1000 psi of steam a refractory cement consisting of a mixture of $CaO:2Al_2O_3$, $CaO:Al_2O_3$, and Al_2O_3 grog might be expected to react slowly at about 450°C. The $3CaO:Al_2O_3:6H_2O$ originally formed in the cement will transform rapidly to form $4CaO:Al_2O_3:3H_2O$, which will then slowly react to form first $12CaO:7Al_2O_3$ plus $CaO:Al_2O_3$ and then eventually $CaO:6Al_2O_3$ plus Al_2O_3.

A similar investigation was conducted in CO_2 under 860 psi. Although insufficient data was collected to construct a phase diagram, the data given in Table 2 indicates that the reactions which occur in a CO_2 environment are similar to those which occur in steam. There are several exceptions. The $4CaO:3Al_2O_3:3H_2O$ at 500°C in steam is stable and under similar conditions

in CO_2 decomposes to $CaCO_3$ and Al_2O_3. Several experiments indicate that other CaO-Al_2O_3 phases may also be stable with respect to the $CaCO_3$-Al_2O_3 system under these conditions.

Two specimens consisting of CA-25 and $4CaO:3Al_2O_3:3H_2O$ were heated in a methane environment at 800°C for two weeks at 1000 psi (Table IV). The x-ray powder pattern of CA-25 (see Table III) showed $CaO:2Al_2O_3$, $CaO:Al_2O_3$, α-Al_2O_3 and an unknown phase (major line ∿24 deg 2θ). The unknown phase does not appear to be calcium formate. The $4CaO:3Al_2O_3:3H_2O$ contains $12CaO:7Al_2O_3$ and $CaO:Al_2O_3$. These are the same reaction products as those occurring under 1000 psi steam at the same composition and temperature.

Four compositions were heated in CO (Table V) at 1000 psi and 700°C for the x-ray pattern of $CaO:Al_2O_3$ showed a mixture of $CaO:Al_2O_3$ and $CaO:2Al_2O_3$ and the $4CaO:3Al_2O_3:3H_2O$ showed the same decomposition products found in the CO_2 and $CaCO_3$. The CA-25 x-ray pattern showed mixtures of $CaCO_3$, α-Al_2O_3, $CaO:2Al_2O_3$ and $CaO:Al_2O_3$ and the $CaO:2Al_2O_3$ showed no reaction.

Conclusions

It is obvious that insufficient experiments have been conducted to make any definitive conclusions. However the following observations should be noted.

1. At 1000 psi steam pressure, the phase boundaries are essentially those which can be predicted from a combination of the published data of Peppler and Wells and Majumdar and Roy.

2. The cementations phases 3:1:6 and 4:3:3 are not stable at any higher temperatures in 1000 psi steam than they are at atmospheric pressure.

3. The compound 4:3:3 decomposes to metastable phases in dry atmospheres such as CO_2 or CO but directly to stable phases in steam.

4. Many of these phases in the $CaO:Al_2O_3:H_2O$ system are not stable in CO_2 (860 psi) with respect to the system $CaCO_3$-Al_2O_3.

In order to determine the possible deleterious effects of the combined gaseous atmosphere present in a coal gasifier considerably more detailed study must be made of this system.

b. Slag-Refractory Interactions

A synthetic slag was formulated by averaging the ash compositions of twelve Pittsburgh coals. (Bur. Mines Bull. 567) with some simplification arrived at the following composition.

SiO_2	49.0% by wt.
Al_2O_3	26.0
Fe_2O_3	19.0
CaO	3.5
MgO	0.7
K_2O	1.2
Na_2O	0.6

A large batch of the above composition was prepared and the viscosity determined over the temperature range 1620 °C to the crystallization temperature of 1470 °C; Figure 3.

A series of magnesium aluminates were prepared in the form of right cylinders 1 cm diameter by 2.5 cm long for immersion in molten slag. The compositions are as follows:

		Density
Al_2MgO_4	Stoichiometric Spinel	3.45 g/cc
90.1 mol% Al_2MgO_4	9.9 MgO	3.40
74.1 Al_2MgO_4	25.9 MgO	3.50
18.6 Al_2MgO_4	81.4 MgO	3.46

A cylinder of stoichiometric magnesium aluminate spinel was immersed in the molten slag to a depth of 3/4 - 1 cm and rotated without reversal at 15 rpm for two hours at a temperature of 1550 °C. The sample was sectioned and visually there was little or no penetration of Fe into the specimen, dissolution was minimal and was estimated to be less than 0.20 mm or 0.1 mm/hr. The same sample examined by SEM did not show any Fe beyond the frozen slag layer, indicating that the degradation process was primarily by solution at the slag-ceramic interface. A sample of 90.1 mole % $MgO.Al_2O_3$-9.9 mole % MgO was subjected to the same slag composition in the same manner for a period of three hours at a temperature of 1575 °C. The cross sectional area had a diffusion layer which could be visually observed as well as the original outline of the sample. The diffusion layer was approximately 1.3 mm thick corresponding to a diffusion rate of 0.13 cm/hr. In a likely manner the end member composition 18.6 mole % $MgO.Al_2O_3$-81.4 mole % MgO was subjected to the slag environment under the same conditions of time, temperature and rotation. The diameter was reduced to 0.778 cm with no obvious diffusion of Fe into the sample. The rate of solution is approximately 0.36 mm/hr. The degradation of the stoichiometric spinel is primarily by solution with a very small diffusion layer. With increasing amounts of MgO first diffusion predominates until the solution rate becomes equal to or greater than the diffusion rate. The obvious conclusion that can be drawn from this is that stoichiometric spinel is more resistant to slag attack than spinel - MgO compositions. From phase considerations one would expect that the stoichiometric spinel would be more resistant than Al_2O_3 under the same conditions.

Plans: The reactions of molten slag with refractories has essentially been discontinued. The effort will be directed toward studying the properties of real and synthetic slags under simulated gasification environments to establish a base of information useful for engineering design.

3. Consultation and Proposal Review

Progress: During the year, thirty proposals were reviewed for ERDA-FE. Six of these proposals were reviewed in the fourth quarter.

Figure 1.

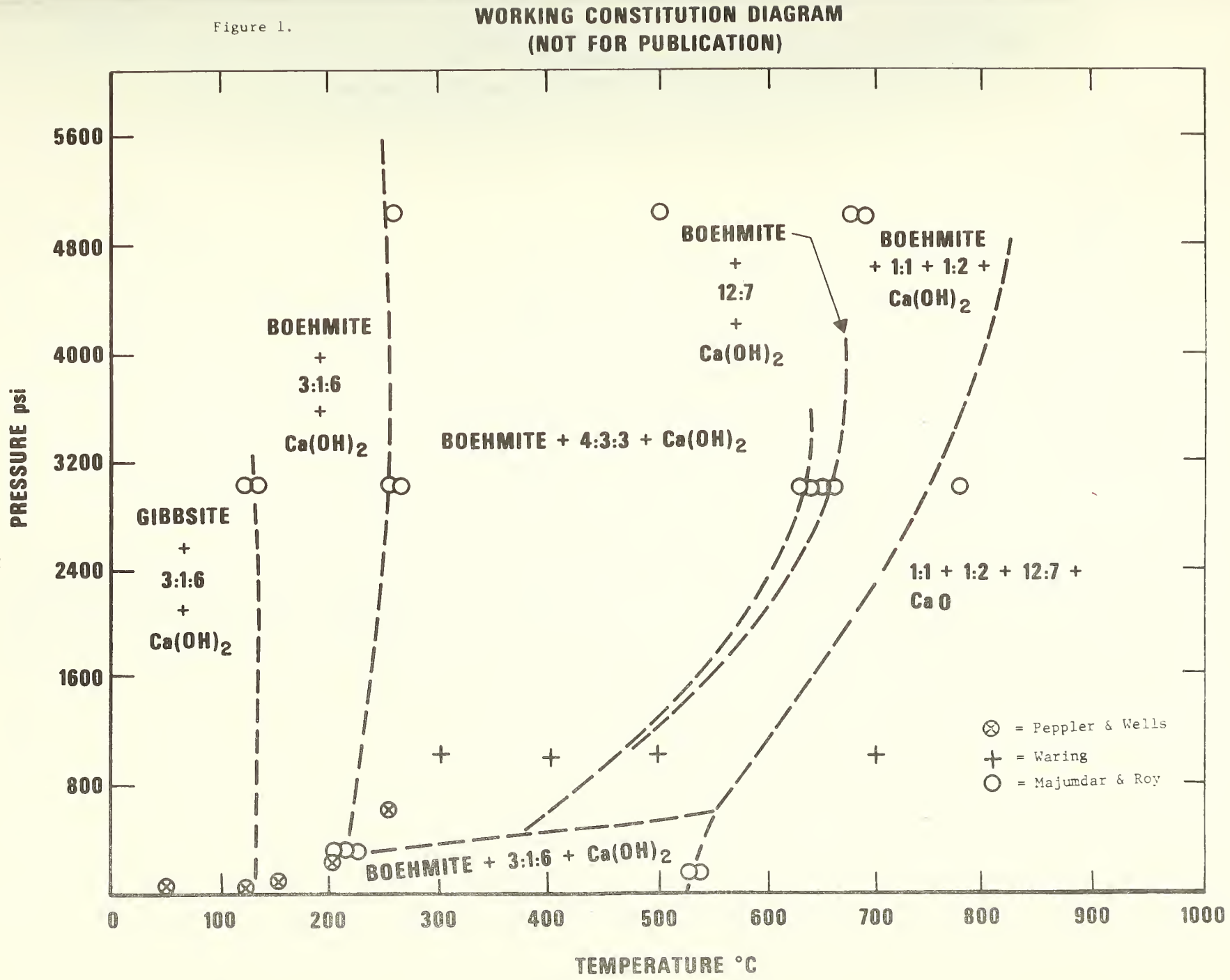
WORKING CONSTITUTION DIAGRAM
(NOT FOR PUBLICATION)
PRESSURE psi
5600
4800
4000
3200
2400
1600
800
0
100
200
300
400
500
600
700
800
900
1000
TEMPERATURE °C
GIBBSITE + 3:1:6 + Ca(OH)2
BOEHMITE + 3:1:6 + Ca(OH)2
BOEHMITE + 4:3:3 + Ca(OH)2
BOEHMITE + 12:7 + Ca(OH)2
BOEHMITE + 1:1 + 1:2 + Ca(OH)2
1:1 + 1:2 + 12:7 + Ca O
BOEHMITE + 3:1:6 + Ca(OH)2
⊗ = Peppler & Wells
+ = Waring
○ = Majumdar & Roy

Figure 2

System $CaO-Al_2O_3-H_2O$

1000 psi

Tentative Constitution Diagram

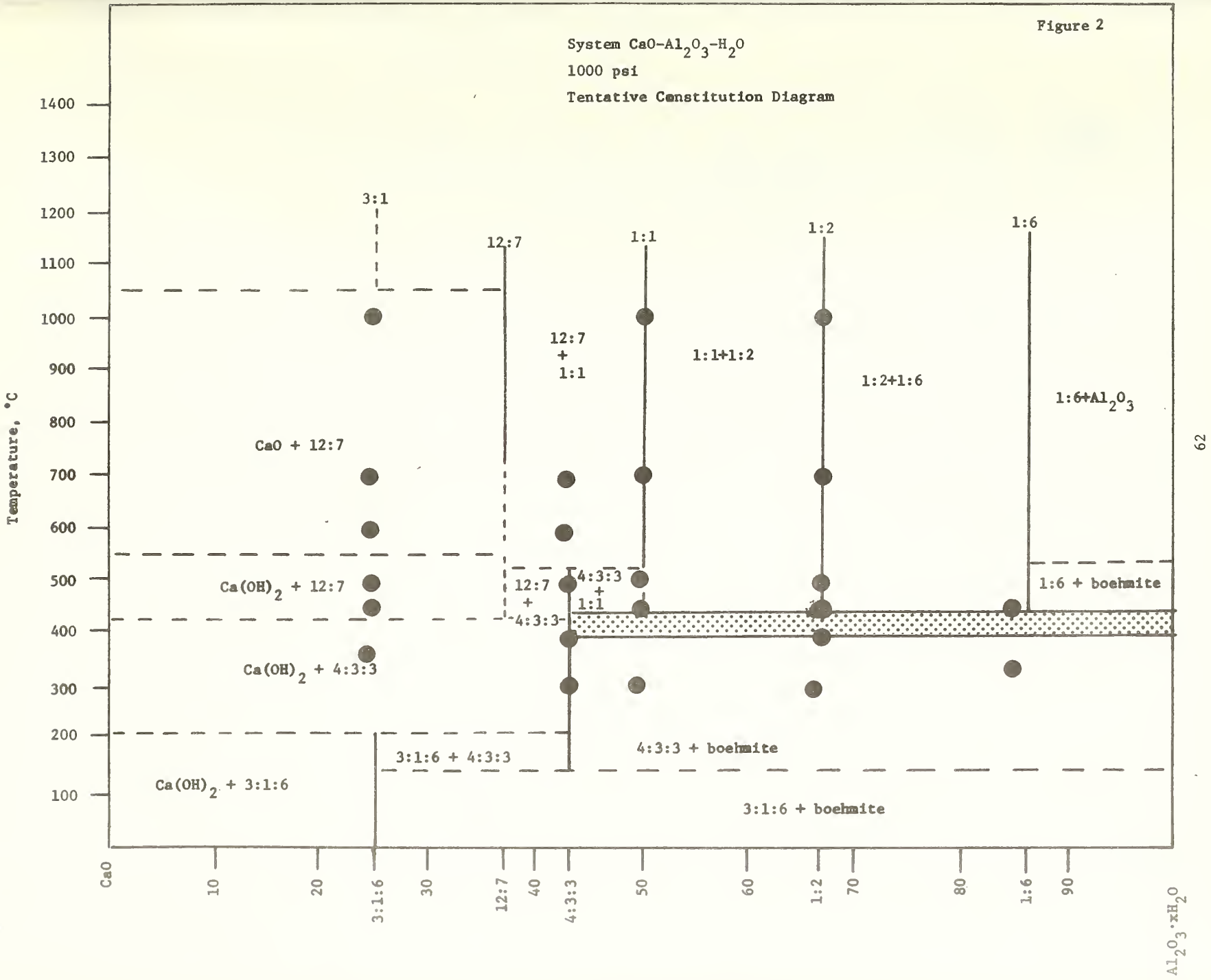

1.5
2.0
2.5
VISCOSITY (Log10 POISES)
1300
1400
1500
1600
1700
TEMPERATURE (C)
1470 ± 5 °C - - - - - - -Approx. Liquidus

Figure 3.

Table 1

Starting Material	Temperature °C	Pressure psi	Time days	X-ray Diffraction Analysis	Conclusion
$CaO:2Al_2O_3$	300	1000	7	$CaO:2Al_2O_3$+$4CaO:3Al_2O_3:3H_2O$+ boehmite	$CaO:2Al_2O_3$ → boehmite + $4CaO:3Al_2O_3:3H_2O$
$CaO:2Al_2O_3$	700	1000	7	$CaO:2Al_2O_3$	$CaO:2Al_2O_3$ → $CaO:2Al_2O_3$
$CaO:Al_2O_3$	700	1000	7	$CaO:Al_2O_3$+trace 1:2(?)	$CaO:Al_2O_3$ → $CaO:Al_2O_3$
$CaO:2Al_2O_3$	400	1000	11	$CaO:2Al_2O_3$+boehmite+ $4CaO:3Al_2O_3:3H_2O$	$CaO:2Al_2O_3$ → boehmite + $4CaO:3Al_2O_3:3H_2O$
$CaO:2Al_2O_3$	500	1000	11	$CaO:2Al_2O_3$	$CaO:2Al_2O_3$ → $CaO:2Al_2O_3$
$CaO:Al_2O_3$	400	1000	11	$CaO:Al_2O_3$	$CaO:Al_2O_3$ (?) experiment must be redone
$CaO:Al_2O_3$	500	1000	11	$CaO:Al_2O_3$ may have faint trace 1:2	$CaO:Al_2O_3$ → $CaO:Al_2O_3$

Table II. Experimental Data for the System $CaO-Al_2O_3-H_2O$ at 1000 psi Steam Pressure.

Starting Material[1/]	Temp. °C	Pressure psi	Time hrs	X-ray Diffraction Analysis	Conclusions
3:1:6	350	1000	720	4:3:3 + $Ca(OH)_2$ + hydrate	3:1:6 → 4:3:3 + hydrate
3:1:6	450	1000	720	4:3:3 + $Ca(OH)_2$ + 3:1:6 + hydrate	3:1:6 → 4:3:3 + hydrate
3:1	350	1000	720	3:1 + $Ca(OH)_2$ + 12:7	3:1 → 12:7 + $Ca(OH)_2$
3:1	450	1000	720	3:1 + $Ca(OH)_2$ + 12:7	3:1 → 12:7 + $Ca(OH)_2$
3:1	500	1000	168	3:1 + 12:7 + $Ca(OH)_2$	3:1 → 12:7 + $Ca(OH)_2$
3:1	600	1000	168	12:7 + 3:1 + CaO	3:1 → 12:7 + CaO
3:1	700	1000	168	3:1 + 12:7 + CaO	3:1 → 12:7 + CaO
3:1	1000	945	120	12:7 + CaO	3:1 → 12:7 + CaO
4:3:3	350	1000	720	4:3:3 + boehmite	$Ca(OH)_2$ + amorphous Al_2O_3 + 4:3:3 → 4:3:3 + boehmite
4:3:3	400	1000	86	4:3:3 + $Ca(OH)_2$	4:3:3 + amorphous $Ca(OH)_2$ + amorphous Al_2O_3 → 4:3:3 + $Ca(OH)_2$
4:3:3	450	1000	720	4:3:3	4:3:3 + amorphous $Ca(OH)_2$ + amorphous Al_2O_3 → 4:3:3
4:3:3	500	1000	86	4:3:3 + $Ca(OH)_2$	4:3:3 + amorphous $Ca(OH)_2$ + amorphous Al_2O_3 → 4:3:3 + cryst $Ca(OH)_2$
4:3:3	500	1000	168	4:3:3	4:3:3 + amorphous Al_2O_3 + amorphous $Ca(OH)_2$ → 4:3:3 + $Ca(OH)_2$
4:3:3	600	1000	168	4:3:3 + 12:7 + CaO	4:3:3 + 12:7 + CaO
4:3:3	700	1000	168	(leaked) 12:7 + 1:1	-----
1:1	300	1000	168	4:3:3 + 1:1 + boehmite	1:1 → boehmite + 4:3:3
1:1	400	1000	240	1:1	1:1
1:1	450	1000	240	1:1 + 4:3:3	1:1 → 4:3:3
1:1	500	1000	264	1:1	1:1 → 1:1
1:1	700	1000	168	1:1 + 1:2	1:1 → 1:1
1:1	1000	945	120	1:1	1:1 → 1:1
1:2	300	1000	168	1:2 + 4:3:3 + boehmite	1:2 → boehmite + 4:3:3 + boehmite
1:2	400	1000	264	1:2 + boehmite + 4:3:3	1:2 → boehmite + 4:3:3
1:2	450	1000	240	1:2	1:2 → 1:2
1:2	500	1000	264	1:2	1:2 → 1:2
1:2	700	1000	168	1:2	1:2 → 1:2
1:2	1000	945	120	1:1	1:1 → 1:2
1:6	350	1000	945	1:6 + 4:3:3 + Al_2O_3	1:6 → 4:3:3 + boehmite + Al_2O_3
1:6	450	1000	945	1:6 + Al_2O_3	1:6 → 1:6 + Al_2O_3

[1/] 3:1:6 = $3CaO:Al_2O_3:6H_2O$
1:2 = $CaO:2Al_2O_3$
3:1 = $3CaO:Al_2O_3$
4:3:3 = $4CaO:3Al_2O_3:3H_2O$
12:7 = $12CaO:7Al_2O_3$
1:1 = $CaO:Al_2O_3$
1:6 = $CaO:6Al_2O_3$

Table III. Experimental Data for Compositions in the System Calcium Oxide (Carbonate) - Aluminum Oxide in 860 psi of CO_2.

Starting Material[a]			Temp.	Pressure	Time	Results[b,c]	Conclusions
						X-ray Diffraction Analysis	
CaO mol%	Al_2O_3 mol%	H_2O mol%	°C	psi	hr		
75	25	0	600	860	72	3:1	3:1 → 3:1
75	25	0	700	860	72	3:1+12:7+$CaCO_3$	3:1 → 12:7+$CaCO_3$
75	25	0	700	860	144	3:1+12:7+$CaCO_3$	3:1 → 12:7+$CaCO_3$
30	10	60	500	860	336	$CaCO_3$+4:3:3	3:1:6 → $CaCO_3$+4:3:3
30	10	60	600	860	384	$CaCO_3$+12:7+1:2	3:1:6 → $CaCO_3$+12:7+1:2
30	10	60	800	860	144	$CaCO_3$+unknown+1:2	3:1:6 → $CaCO_3$+unknown[d]+1:2
40	30	30	500	860	288	4:3:3+Al_2O_3+$CaCO_3$	4:3:3 → $CaCO_3$+Al_2O_3
40	30	30	600	860	384	unknown[d]+$CaCO_3$	4:3:3 → unknown[d]+$CaCO_3$
40	30	30	700	860	144	1:1+$CaCO_3$+unknown[d]	4:3:3 → 1:1+$CaCO_3$+unknown[d]
40	30	30	800	860	144	1:1+1:2+$CaCO_3$+unknown[d]	4:3:3 → ?
50	50	0	500	860	288	1:1+Al_2O_3+$CaCO_3$	1:1 → Al_2O_3+$CaCO_3$
50	50	0	600	860	72	1:1	1:1 → 1:1
50	50	0	700	860	72	1:2+$CaCO_3$	1:1 → 1:2+$CaCO_3$
50	50	0	800	860	144	1:1	1:1 → 1:1
33.33	66.67		500	860	720	1:2	1:2 → 1:2
			700	860	192	1:2	1:2 → 1:2
1.4285	85.715		500	860	720	1:6+tr+α-Al_2O_3	1:6 → 1:6

[a] All bulk starting materials which were spectrographic pure were mixed and were calcined at sufficient time and temperature to obtain single phase materials. These specimens were heated in a conventional hydrothermal bomb in open Pt tube and were quenched by water emersion from the temperatures indicated.

[b] The phases identified are given in order of the amount present (greatest amount first) at room temperature. These phases are not necessarily those present at the temperature to which the specimen was heated.

c/ The following short notations were used for clarity:

3:1 = $3CaO:Al_2O_3$

3:1:6 = $3CaO:Al_2O_3:6H_2O$

12:7 = $12CaO:7Al_2O_3$

4:3:3 = $4CaO:3Al_2O_3:3H_2O$

1:1 = $CaO:Al_2O_3$

1:2 = $CaO:2Al_2O_3$

1:6 = $CaO:6Al_2O_3$

d/ An unknown dehydration product.

Table IV. Experimental Data for Compositions in the System Calcium Oxide (Carbonate) - Aluminum Oxide in Methane.

Starting Materials[a]	Temp. °C	Pressure psi	Time hr	Results[b] X-ray Diffraction Analysis	Conclusions
CA-25	800	1000	316	$CaO:2Al_2O_3$+$CaO:Al_2O_3$+α-Al_2O_3 +unknown[c]	
$4CaO:3Al_2O_3:3H_2O$	800	1000	316	$12CaO:7Al_2O_3$+$CaO:Al_2O_3$	$4CaO:3Al_2O_3:3H_2O \rightarrow$ $12CaO:7Al_2O_3$+$CaO:Al_2O_3$

[a] All bulk starting materials which were spectrographic pure were calcined at sufficient time and temperature to obtain single phase materials. These specimens were heated in an open platinum tube in a conventional hydrothermal bomb.

[b] The phases identified are given in order of the amount present (greates amount first) at room temperature. These phases are not necessarily those present at the temperature to which the specimen was heated.

[c] Specimen contains an unknown phase with the major x-ray diffraction powder line occurring at about 24 deg 2θ.

Table V. Experimental Data for Compositions in the System Calcium Oxide (Carbonate) - Aluminum Oxide in Carbon Monoxide.

Starting Materials[a]	Temp. °C	Pressure psi	Time hr	Results[b] X-ray Diffraction Analysis	Conclusions
$CaO:Al_2O_3$	700	1000	110	$CaO:Al_2O_3$+$CaO:2Al_2O_3$	
$4CaO:3Al_2O_3:3H_2O$	700	1000	110	$CaO:Al_2O_3$+unknown[c] +$CaCO_3$	$4CaO:3Al_2O_3:3H_2O \rightarrow CaO:Al_2O_3$ +$CaCO_3$+unknown
$CaO:2Al_2O_3$	700	1000	110	$CaO:2Al_2O_3$	$CaO:2Al_2O_3 \rightarrow CaO:2Al_2O_3$
CA-25	700	1000	110	$CaCO_3$+α-Al_2O_3+$CaO:2Al_2O_3$ +$CaO:Al_2O_3$	--

[a] All bulk starting materials which were spectrographic pure were calcined at sufficient time and temperature to obtain single phase materials. These specimens were heated in an open platinum tube in a conventional hydrothermal bomb.

[b] The phases identified are given in order of the amount present (greatest amount first) at room temperature. These phases are not necessarily those present at the temperature to what the specimen was heated.

[c] A unknown dehydration product.

4. Failure Analysis (J. H. Smith, 312.01)

A. Failure Avoidance Program

Progress: Additional reports of pilot plant operating discrepancies and component failure have been received during this quarter. Approximately 250 items of information have been received from nine different pilot plants and process development units. All of this information has been evaluated, classified, and abstracted for inclusion in the Failure Avoidance Program data base.

As part of the information collection phase of this task, visits were made to the ERDA-Synthane pilot plant, Bigas pilot plant, and the Westinghouse combined-cycle pilot plant at Waltz Mills. The operating experiences and component failures experienced to date were reviewed with the plant operating personnel at these pilot plants. At present, the Bigas Pilot Plant has not started operation, so no information was received from this source, but arrangements were made to receive available information on component failures when operation of the plant is started. The Synthane plant has had limited operation of some subsystems which resulted in a few shutdowns due to component failures. Details of these failures were reviewed and the information in the Failure Avoidance Program data base were brought up-to-date. The Westinghouse-Waltz Mills pilot plant has a very detailed system for documentation of operating discrepancies and component failures. This system was reviewed in detail and arrangements were made to study the information available from this source.

Additional information collection activities included attending the American Society for Metals Conference entitled "Materials for Coal Conversion Systems Design" on April 26 and 27, 1976 in Pittsburgh, Pennsylvania. In addition, activities of the Metals Properties Council Committee on Materials for Coal Conversion were participated in.

The evaluation, classification, and preparation of detailed abstracts has been completed for all information received to date from the pilot plants. An automated, computer based data system has been established and developed to permit efficient storage and retrieval of all information included in the data base. At present, all available extended abstracts and classification of information items has been put on this system. The use of this system is being refined and training of personnel in its use is continuing. The use of this system will permit rapid and efficient access to all failure avoidance information and will permit failure mode analysis programs to be conducted.

As part of the information dissemination phase of this task, a presentation entitled "The ERDA-Fossil Energy Failure Avoidance Program" was presented at the Mechanical Failures Prevention Group Meeting on "Prevention of Failures in Coal Conversion Systems" in Columbus, Ohio. In addition, a

summary of results obtained to date was published in the April 1976 issues of the ERDA-Materials and Components Newletter.

A presentation was made to explain the use of the Failure Avoidance Program at the annual GIDEP information meeting on May 27 in Alexandria, Virginia. In addition, the possible use of the GIDEP system for future use in the Failure Avoidance Program was explored.

Plans: The information gathering phase of this task will continue as more information is received on a continuing basis from the pilot plants. In addition, detailed follow-up of certain information already received will be initiated. Additional visits to operating pilot plants will be made to collect additional information.

The information evaluation and proce-s phase of this program will continue and be enlarged. The operation of the automated data storage system will be enlarged and refined for easier and more efficient use. The information presently in the data base will be used to conduct failure mode analyses to identify critical operating problem areas.

The information dissemination phase of this program will continue and will be developed to include more direct contact with users. At present, several inquiries a month are answered from plant operations and design personnel. Plans have also been initiated to include summary results of this program in the bimonthly ERDA-Materials and Components Newsletter.

Additional information dissemination will take place through the Fossil Energy - Performances Assurance Systems that is currently under development. Close liaison with this program is being maintained.